Journal of Marine Science and Application (2025) 24: 998-1018
https://doi.org/10.1007/s11804-025-00704-6

RESEARCH ARTICLE

Effect of Seabed Geometry on the Hydrodynamic Performance of a Thick Wavy Porous Barrier

V. Venkateswarlu[1], D. Suresh Kumar[2], I. Srinivasula Reddy[3] and S. C. Martha[4]

Received: 13 June 2024 / Accepted: 08 March 2025

Abstract

This study evaluates the physical mechanisms of incident waves as they interact with a porous wavy barrier of finite thickness. A wave-trapping chamber is formed between the thick wavy barrier (TWB) and partially reflecting seawall (PRS). The effect of seabed undulations is incorporated into the wave-trapping analysis of the TWB. The boundary value problem proposed in this study is solved using a multidomain boundary element method within the context of linear potential flow theory. Coefficients such as reflection, runup, horizontal force on PRS, and vertical force on TWB are examined for various structural configurations. The position of seabed undulations is analyzed for four scenarios: i) seabed undulations upwave of the wavy barrier with a trapping chamber, ii) seabed undulations upwave of the wavy barrier without a trapping chamber, iii) seabed undulations underneath the wavy barrier with a trapping chamber, and iv) seabed undulations beneath the wavy barrier without a trapping chamber. The study results are compared with known results to verify their accuracy. The effects of PRS, TWB porosity, trapping chamber, plate thickness, seabed type, and submergence depth on hydrodynamic coefficients are analyzed against relative water depth. The study reveals that the introduction of a porous TWB with a trapping chamber results in minimal hydrodynamic coefficients (reduced reflection and force on a wall) compared to a rigid TWB without a trapping chamber. A comparison of various seabeds is reported for all combinations of TWB with a chamber. The sloping seabed upwave of the barrier with a trapping chamber, 20% plate porosity, and 50% wall reflection at an appropriate submergence depth could replace gravity-type breakwaters in deeper waters. This study holds great potential for analyzing wave trapping coefficients by TWB to provide an effective coastal protection system.

Keywords Wave trapping; Thick wavy plate; Porosity; Partially reflecting wall; Multidomain boundary element method; Undulated seabed

1 Introduction

Various wave energy absorbers, such as rubble-mound structures (Sollitt and Cross, 1972), pile-rock breakwaters (Nguyen et al., 2022), floating docks (Vijay et al., 2021), T-type (Neelamani and Rajendran, 2002), H-type (Nishad et al., 2021), multilayered thick or thin vertical porous structures (Venkateswarlu and Karmakar, 2020), and horizontal and inclined porous plates (Cho and Kim, 2008), have been recommended by several researchers to minimize wave action near the shoreline. Rubble mounds offer several advantages for shoreline stabilization against wave action but also have some notable disadvantages. These fully extended structures (seabed to the free surface) partially obstruct free water circulation and sediment transport, interrupt fish migration, and restrict various developmental and tourism activities. Similarly, submerged rubble-mound breakwaters are more effective than fully extended breakwaters, but they concentrate most of the wave energy near the mean free surface. Thus, coastal countries have introduced inclined or horizontal floating thin plates to create a tranquil wave climate. However, floating thin plates offer temporary protection against incident waves with moderate to minimal wavelengths. Therefore, coastal communities urgently require structures with enhanced hydrodynamic performance and minimal negative environmental impact. In the preliminary

Article Highlights

- Sinusoidal ripples are introduced for a horizontal plate of finite thickness.
- Zero minima of wave reflection are observed by thick wavy plate when relative water depth approaches $k_0h = 1.6$ and $k_0h = 3$.
- The well-balanced trapping and force coefficients are obtained for sloppy seabed with wavy barrier.

✉ V. Venkateswarlu
venki@nitsri.ac.in

[1] Department of Civil Engineering, National Institute of Technology Srinagar, Srinagar, Jammu and Kashmir 190006, India

[2] TechnipFMC Technologies India Private Limited, Hyderabad, Telangana 500039, India

[3] Department of Civil Engineering, KSRM College of Engineering, Kadapa, Andhra Pradesh 516003, India

[4] Department of Mathematics, Indian Institute of Technology Ropar, Rupnagar, Punjab 140001, India

stage, porous plates of finite thickness were introduced to address incident wave action (Liu et al., 2012). To further enhance the hydrodynamic performance of thick porous plates, sinusoidal ripples were introduced in the second stage. The wave reflection performance of thick wavy plates is effective compared to horizontally thick plates, while the performance of horizontally thick plates is notable compared to thin plates. However, seabed changes are frequently observed in several coastal regions (Kaligatla et al., 2018; Tabssum and Ramakrishnan, 2024). Thus, this study considers the effect of seabed undulations on the wave trapping analysis of thick wavy plates. The effects of seabed undulations i) upwave and ii) underneath thick wavy plates on wave trapping and force coefficients are analyzed using the multidomain boundary element method (MBEM).

The hydrodynamic performance of horizontal plates was first analyzed by Heins (1950) for intermediate waves. Subsequently, various researchers reported their opinions on the performance evaluation of horizontal plates when submerged in an infinite depth (Greene and Heins, 1953; Burke, 1964; Leppington, 1972). Siew and Hurley (1977) proposed a mathematical model to analyze wave scattering by horizontal plates for long waves. Their study presented the variation in wave reflection against the relative wavenumber. The variation in energy flux around horizontal plate breakwaters was examined by Patarapanich (1984) for deeply submerged conditions. The magnitude of the oscillatory or sloshing peaks may be reduced when the rigid plate is replaced with the porous plate (Choudhary and Martha, 2023). The reflected wave energy by the thick plate again interacts with the incoming wave energy (Patarapanich and Cheong, 1989), and the resultant wave field in the seaside region is a superposition of multiple waves. Hence, the ultimate wave reflection by the thick plate results from the phase difference. The reflection is maximum when all the waves follow the same phase and minimal or almost zero when they are in the opposite phase (Patarapanich, 1984), owing to the formation of standing waves.

Several analytical, numerical, and experimental studies (Davies, 1982; Mondal et al., 2017; Venkateswarlu and Karmakar, 2020; Varghese et al., 2024; Vishwakarma and Karmakar, 2024) have incorporated the effect of seabed undulations on wave scattering and trapping. From a field perspective, seabed undulations are responsible for fluid resonance, which is observed in scattering, trapping, and force coefficients (Kaligatla et al., 2018). Seabed undulations enhance the efficiency of onshore and offshore wave energy converters (Rezanejad et al., 2015; Ning et al., 2016). Chwang (1983) introduced the porous wave-maker theory, which considers a vertical permeable wall against incident waves. Yu and Chwang (1994) investigated wave motion in the presence of a submerged porous plate, focusing on variations in wave reflection and transmission against incident wave properties. Zero wave reflection and transmission were observed because of the phase change of the incident wave after interacting with the submerged plate. To date, hydrodynamic studies have focused on fixed plates, and Yip and Chwang (1997) added the property of pitching to submerged plates. The pitching plate comprises some initial motion, and the movement of the plate (up and down) either enhances wave reflection (sometimes more than unity) or reduces wave transmission (varying from 0 to 2). Rageh et al. (2009) experimentally examined the performance of partially submerged breakwaters with supporting piles. Behera et al. (2015) evaluated the performance of submerged flexible porous plates against incident waves. Zhang et al. (2018) discussed viscous flow in the presence of an inverted π-type breakwater under incident waves.

Furthermore, Cho and Kim (2000) evaluated the wave scattering performance of horizontal flexible plates using linear hydroelastic theory, applying the coupled MBEM and enhanced finite element method (EFEM) to the plate and outer regions, respectively. The study results were verified through laboratory measurements, and membrane porosity demonstrated a considerable impact on dissipating incident wave energy. Yu (2002) provided a detailed review of horizontal plate breakwater and its various effects, such as plate length, porosity, inclination, width, submergence depth, plate vibration, fluid viscosity, current presence, wave irregularity, and nonlinearity, as well as the historical development of breakwater on wave scattering coefficients. Cho and Kim (2008) expanded on their previous study by incorporating the membrane's inclination, with the membrane backed by a rigid wall. The study results were verified with the independently measured values in the wave flume laboratory. Yueh et al. (2016) proposed single, double, and triple wavy plates of uniform amplitude and wavy plates of multiple ripples with nonuniform amplitudes as potential wave decomposers using the dual boundary element method (DBEM). Dai et al. (2018) provided a review of research on the development of various types of floating breakwaters, including (a) box, (b) pontoon, (c) frame, (d) mat, (e) tethered float, and (f) horizontal plate, and their impact on incident wave scattering. Venkateswarlu et al. (2021) investigated the trapping of incident waves by a wavy plate with nonidentical ripples using the DBEM. The wavy plate was installed far from the partially reflecting inclined seawall, and the numerical study suggested that 20% plate porosity with 50% wall reflection to achieve the well-balanced trapping and force coefficients. Kumar et al. (2023) compared the wave scattering performance of bottom-standing porous structures when integrated with horizontal thin plates of (a) zero porosity and (b) porosity with flexible properties. Fluid resonance occurs when the plate is nonporous, and upon introducing porosity, the oscillatory scattering coefficients are minimized owing to improved wave damping. Mohapatra and Sahoo (2023) examined surface gravity wave scattering by a composite wavy barrier in the pres-

ence of a floating dock using the MBEM. The composite wavy plate produced a nearly zero value of wave transmission compared to the submerged horizontal plate and floating dock.

Thin breakwaters, such as thin-wall barriers and horizontal plate breakwaters, are suitable for providing temporary protection against incident waves with moderate to minimal wavelengths (Evans and Peter, 2011; Koley et al., 2015). However, these structures are unsuitable for withstanding waves with higher wavelengths owing to their limited thickness. Thus, to improve the wave scattering and trapping capabilities of these thin-wall structures, researchers have introduced the plate thickness. Liu and Iskandarani (1991) investigated horizontal plates of finite thickness to define wave reflection and transmission using the EFEM, aiming to protect shelter regions from long, intermediate, and shorter waves. The performance of thick plates was particularly effective in controlling short waves. However, the authors observed harmonic resonance in the sheltered regions when the thick plate interacted with waves of high wavelengths. Liu et al. (2012) added the property of porosity for thick horizontal breakwaters, as discussed by Liu and Iskandarani (1991). The EFEM, which comprises symmetric (antisymmetric) parts, is incorporated to simplify the complex plate dispersion relation, and the study results are validated with independently developed MBEM results. Bautista et al. (2022) proposed a pair of submerged, floating, thick-plate breakwaters with wavy surfaces as a potential breakwater against incident waves. Wave scattering coefficients were reported using a mathematical model with patching boundary conditions. Wavy ripples are sinusoidal and designed to enhance fluid–particle interaction with the breakwater, leading to maximum wave reflection and minimal wave transmission. These structures would replace the gravity-type rubble-mound breakwaters owing to their improved performance. The magnitude of wave reflection by the twin-plate breakwater system increases with the introduction of third-order wavy surfaces. Beyond this point, the magnitude of the wave reflection becomes minimal. From an application viewpoint, slender piles will be used to install the wavy structure at the proposed location.

This study examines the physical mechanism of wave trapping by a thick, wavy plate in the presence of a partially reflecting seawall (PRS). To the author's knowledge, wave trapping analysis of a thick wavy barrier (TWB) installed over an undulated seabed and away from it is rarely reported. The wavy structure is slightly thicker than the conventional horizontal or vertical plates, which comprise mesh-type porous material. This study primarily aims to demonstrate the effectiveness of wavy surfaces in enhancing wave reflection. The presentation is organized as follows: Section 1 provides a general introduction and reviews the literature on vertical, horizontal, thin, and thick plates. Section 2 outlines the mathematical formulation, and Section 3 presents the solution method used based on the MBEM. Section 4 provides verification of the study's numerical results and analyzes the effect of various properties of a thick wavy plate, including wall reflection, plate porosity, thickness, submergence depth, and chamber spacing, against the relative water depth. This analysis is conducted for seabed undulations located i) upwave of the wavy barrier with a trapping chamber, ii) upwave of the wavy barrier without a trapping chamber, iii) underneath the wavy barrier with a trapping chamber, and iv) underneath the wavy barrier without a trapping chamber. Section 5 concludes the study outcomes for further research on the wave trapping analysis of thick plates of wavy surfaces.

2 Mathematical formulation

Incident wave trapping by a wavy barrier of finite thickness placed on an undulated seabed is examined under the assumption of linear potential flow theory. The thick plate comprises sinusoidal oscillations, and a finite trapping chamber is provided between the seawall and barrier. The property of partial reflection is incorporated to control waves of higher wavelengths. An oblique wave interacts with the TWB, and the y-axis is considered vertically positive upward, while the x and z axes are aligned along the horizontal directions in the three-dimensional Cartesian coordinate system. The origin is chosen at the mean free surface, as shown in Figures 1(a) and 1(b). Different structural configurations are evaluated, including seabed undulations: i) upwave of the wavy barrier with the trapping chamber, ii) seabed undulations upwave of the wavy barrier without the trapping chamber, iii) seabed undulations underneath the wavy barrier with the trapping chamber, and iv) seabed undulations underneath the wavy barrier without the trapping chamber. The various seabed profiles analyzed in this study are reported in Figure 2. Some assumptions are made while analyzing the boundary value problem (BVP) involving the incident wave and TWB. The TWB is submerged at a fixed point using slender piles, and the effect of the slender piles on the trapping coefficients is neglected. Furthermore, the TWB porosity is identical.

The study considers that the fluid is incompressible and inviscid and that the motion is irrotational and simple harmonic in time with angular frequency ω. Hence, a velocity potential $\Phi(x,y,z,t)$ exists in the form $\Phi(x,y,z,t) = \mathrm{Re}\left\{\phi(x,y)\mathrm{e}^{-\mathrm{i}(lz-\omega t)}\right\}$, where $l = k_0\sin\theta$ is the wavenumber component in the z-direction, k_0 represents wavenumber in the y-direction, θ denotes the angle of wave contact with breakwater, and Re represents the real part of the spatial complex potential $\phi(x,y,z)$, which satisfies the Helmholtz equation:

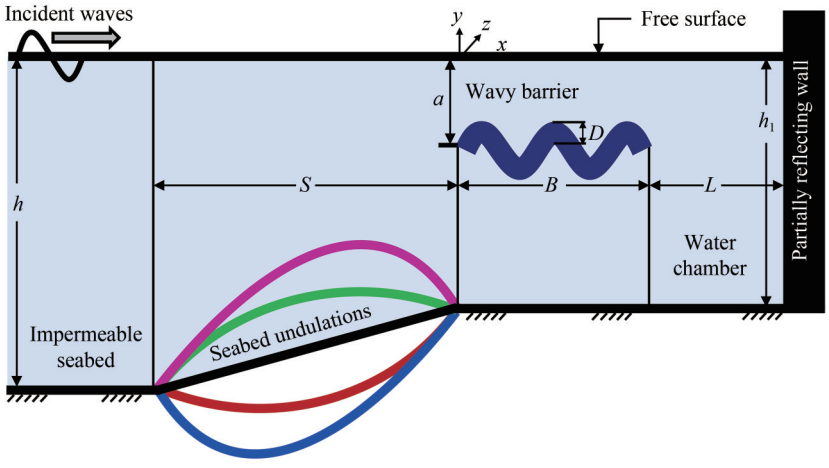

(a) Wavy plate placed away from bottom undulation

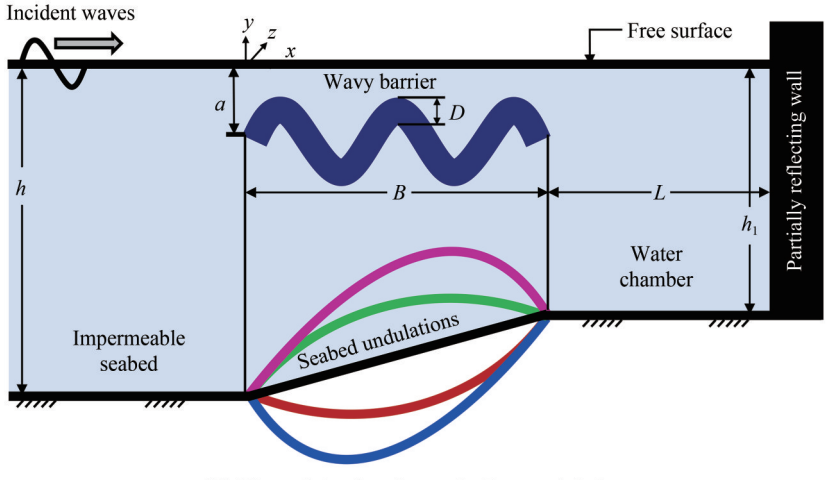

(b) Wavy plate placed upon bottom undulation

Figure 1 Wavy plate of finite thickness placed

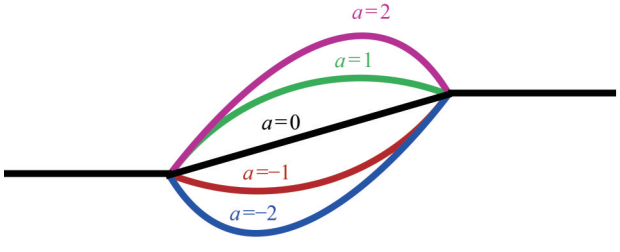

Figure 2 Various types of seabed undulations examined in this study

$$\frac{\partial^2\phi}{\partial x^2}+\frac{\partial^2\phi}{\partial y^2}-l^2\phi=0 \tag{1}$$

The free surface boundary condition in the linearized form is given by:

$$\frac{\partial\phi}{\partial y}-\frac{\omega^2}{g}\phi=0,\ \text{on}\ y=0,\ -\infty<x<(B+L) \tag{2}$$

The zero-velocity condition along the seabed in the presence of a sloping seabed is given by:

$$\frac{\partial\phi}{\partial n}=0,\ -\infty<x<\infty\ \text{and}\ y=-h \tag{3}$$

The condition of a PRS (Isaacson and Qu, 1990; Zhao et al., 2016; Appandairaj et al., 2024), which includes the seawall reflection property, is given by:

$$\frac{\partial\phi}{\partial y}=\mathrm{i}k_0\left(\frac{1-C_R}{1+C_R}\right)\phi \tag{4}$$

where k_0 is the incident wavenumber in y-direction and C_R represents the wave reflection property of the seawall, which varies within $0 \leqslant C_R \leqslant 1$. The $C_R = 0$ indicates that the wall is transparent to incident waves and $C_R = 1$ implies that the wall reflects the total wave energy approached after TWB.

The horizontal plate has a finite thickness, so the fluid flow through the plate follows Darcy's law of motion. The

velocity and pressure continuity across the plate in the vertical direction are given by Sollitt and Cross (1972):

$$\frac{\partial \phi^-}{\partial n} = -\mu \frac{\partial \phi^+}{\partial x} \text{ and } \phi^- = (m + \mathrm{i}f)\phi^+ \tag{5}$$

where superscripts − and + demonstrate flow between the open water and TWB in the vertical and horizontal directions, respectively; $(m + \mathrm{i}f)$ represents the impedance of the porous medium, with m and f being the inertia and friction factors associated with the porous medium, respectively; $\mathrm{i} = \sqrt{-1}$ is the imaginary term; and μ represents the TWB porosity, which varies from 0 to 1. The inertia offered by the TWB is given by:

$$m = 1 + A_m\left[\frac{1-\mu}{\mu}\right] \tag{6}$$

where A_m denotes the added mass coefficient and is negligible as the plate is fixed at a particular point. After substituting $A_m = 0$, the inertia coefficient approaches unity and is kept fixed throughout the study (Dalrymple et al., 1991; Vijay et al., 2020). The friction by the TWB is identified using the following relation (Pérez-Romero et al., 2009):

$$f = f_c\left(Dk_0\right)^{-0.57} \tag{7}$$

where f_c is a constant that varies within the range of $0.21 \leqslant f_c \leqslant 0.46$, and the near mid-value $f_c = 0.31$ is considered and kept fixed throughout the study. D represents the characteristic pore diameter and k_0 is the wavenumber, which satisfies the dispersion relation $\omega^2 = gk_0\tanh\left(k_0h\right)$.

The property of sinusoidal ripples (sine curve) for a wavy barrier is expressed as:

$$P(x) = -a + r_a\sin\frac{\pi d}{B}\left(x + \frac{B}{2}\right), \text{ for } -B/2 \leqslant x \leqslant B/2 \tag{8}$$

Various seabed profiles (Behera and Ghosh, 2019; Panduranga et al., 2023) are examined to evaluate the performance of TWB using the following relation:

$$h(x) = h - b\left\{1 - \alpha(1 - x/S)^2 + (\alpha - 1)(1 - x/S)\right\} \tag{9}$$

where $b = (h - h_1)$, $h(x)$ is seabed function, and α represents the various kinds of seabed profiles, as discussed in Figure 2.

The velocity potentials in the seaward and leeward unbounded outer regions are given by:

$$\phi = \frac{\mathrm{i}gH}{2\omega}\left[\mathrm{e}^{\mathrm{i}k_{0x}(x+L)}Y_0(y) + R_0\mathrm{e}^{-\mathrm{i}k_{0x}(x+L)}Y_0(y)\right], x \leqslant -M \tag{10}$$

where M is assumed to maintain a sufficiently large distance with the breakwater ($M \geqslant 5h$), and R_0 represents the amplitude of the reflected wave. The vertical eigenfunction $Y_0(y)$ in Eq. (10) is expressed as follows:

$$Y_0(y) = \frac{\cosh\left(k_0(y-h)\right)}{\cosh\left(k_0h\right)} \tag{11}$$

The effect of evanescent wave modes on the hydrodynamic coefficients is neglected as the TWB is positioned at a sufficiently large distance from the shoreline and fixed at ($M \geqslant 5h$), following the recommendations of Mackay and Johanning (2020). Moreover, the pressure and velocity are assumed to be continuous on fictitious boundaries. Multiplying both sides of Eq. (10) by $Y_0(y)$ and integrating from $-h$ to 0 yields the following:

$$R_0 = \frac{2\mathrm{i}\omega}{gHN_0^2}\left[\int_{-h}^{0}\phi Y_0(y)\mathrm{d}y\right] - 1 \tag{12}$$

where $N_0^2 = \int_0^h Y_0^2(y)\mathrm{d}y$. The leeside of the breakwater is occupied by a PRS, causing the transmitted wave energy from the sinusoidal barrier to interact with the seawall. The seawall then reflects the energy toward the seaside, resulting in wave reflection in the presence of the back wall with the breakwater. The reflection coefficient K_R is a measure of reflected wave height to incident wave height and is given by:

$$K_R = |R_0| \tag{13}$$

3 Numerical solution using MBEM

This study explores water wave trapping by a TWB over an undulating seabed with nonrectilinear boundaries. Thus, the use of analytical or semianalytical methods involves several higher-order relations, making it cumbersome to identify the coefficients. Therefore, MBEM is adopted to solve the BVP, simplifying the solution method for various nonrectilinear boundaries. Figure 3 shows the computational domain, where the fundamental solution and Green's second identity serve as the foundation of the MBEM. Mathematically, this is expressed as follows:

$$\beta^j(p)\phi^j(p) = \int_{\Gamma^j}\left(\phi^j(q)\frac{\partial G^j(q,p)}{\partial n^j} - G^j(q,p)\frac{\partial \phi^j(q)}{\partial n^j}\right)\mathrm{d}\Gamma^j(q) \tag{14}$$

where $j = 1, 2$ are the computational domains under consideration.

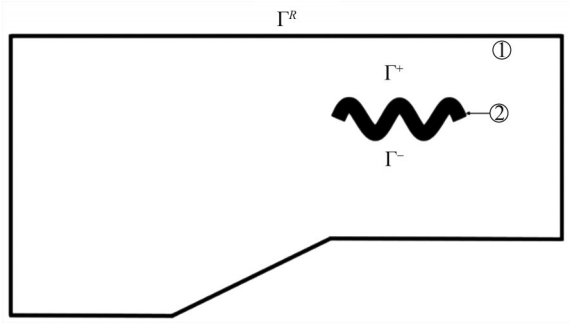

Figure 3 Computational domain of the proposed physical problem

The free-term coefficient $\beta^j(p)$ is defined by:

$$\beta^j(p)=\begin{cases}1, & \text{if } p\in\Omega\\ \dfrac{1}{2}, & \text{if } p\in\Gamma\,(\text{smooth})\\ 0, & \text{if } p\notin\Omega+\Gamma\end{cases} \tag{15}$$

where Ω represents the computational domain, whereas Γ denotes the boundary of the computational domain. The fundamental solution G^j (also known as free-space Green's function) and its normal derivative $\dfrac{\partial G^j}{\partial n^j}$, corresponding to the modified Helmholtz equation in two dimensions, are enforced by:

$$G^j=-\frac{1}{2\pi}K_0(lr),\frac{\partial G^j}{\partial n^j}=\frac{l}{2\pi}K_1(lr)\frac{\partial r}{\partial n} \tag{16}$$

where K_0 and K_1 are the modified Bessel function of the second kind of zeroth order and first-order, respectively, and $r=|q-p|=\sqrt{(x-x_0)^2+(y-y_0)^2}$ is the distance between the field point $q=(x,y)$ and the source point $p=(x_0,y_0)$.

Obtaining an analytical solution to Eq. (14) is generally impractical for problems involving irregular geometry and complex boundary conditions. In such cases, a numerical approximation of the computational domain's boundary is necessary. Therefore, the entire boundary is discretized into N^j constant elements. We assume that the velocity potential and its normal derivate (flux) are constant over each element. Applying the discretized form of Eq. (14) at the midpoint of each element and using Eqs. (2)–(11) yields a system of linear algebraic equations:

$$\sum_{q=1}^{N^j}\frac{\partial\phi_q^j(q)}{\partial n^j}\left[\int_{\Gamma_q^j}G_q^j(q,p)\,\mathrm{d}\Gamma_q^j(q)\right]=\sum_{q=1}^{N^j}\phi_q^j(q)\left[\int_{\Gamma_q^j}\frac{\partial G_q^j(q,p)}{\partial n^j}\,\mathrm{d}\Gamma_q^j(q)-\beta_q^j(p)\right] \tag{17}$$

The superscripts illustrate the domain, and the subscripts signify the boundary element of the jth domain. We used the numerical Gaussian quadrature method to evaluate the boundary integrals (influence coefficients) in Eq. (16). For further details, refer to Vijay et al. (2021). Various unknown coefficients of engineering interest (wave scattering and trapping coefficients) are computed after obtaining the unknown potentials. The time-independent nondimensional horizontal force on the barrier X_W, vertical force coefficient on the wall Y_P, and wave runup coefficient K_H are identified using the following relations:

$$\text{Horizontal force on the wall } X_W=\frac{\left|\oint p(x,y)\,n_x\,\mathrm{d}\Gamma\right|}{\rho gHh} \tag{18}$$

$$\text{Vertical force on wavy plate } Y_P=\frac{\left|\oint p(x,y)\,n_y\,\mathrm{d}\Gamma\right|}{\rho gHh} \tag{19}$$

$$\text{Wave runup } K_H=\frac{2|\eta|}{H}\text{ or }K_H=\frac{2|\mathrm{i}\rho\omega\varphi|}{gH} \tag{20}$$

where $p(x,y)$ represents the hydrodynamic pressure given as

$$p(x,y)=\mathrm{i}\rho\omega\varphi \tag{21}$$

4 Results and discussion

In this study, the trapping of incident waves by a TWB with PRS is reported in the presence of seabed undulations. Prior to the numerical analysis, the verification of the numerical results is presented against the available results. Thereafter, coefficients, including reflection, runup, horizontal force PRS, and vertical force on the TWB, are reported against relative water depth.

4.1 Verification of the study results

Verifying predicted results is essential for further developing the study outcomes and conclusions. Thus, the results are verified with readily available numerical and experimental data from renowned researchers. Liu et al. (2012) developed a semianalytical method to solve engineering quantities when a submerged horizontal thick barrier (HTB) is installed in water of finite depth.

Figure 4(a) shows the wave reflection K_R and transmission K_T by the HTB in the absence of a seawall when $B/h=1$, $D/h=0.1$, $f=2$, and $\mu=0.45$. The linear increment of submergence depth drastically maximizes the K_T, with K_R being the least affected. Figure 4(b) demonstrates the K_R by an HTB attached to a vertical seawall when $a/h=0.1$, $D/h=0.1$, $f=2$ and $\mu=0.45$. In both cases, this

study's results parallel those reported by Liu et al. (2012) for wave scattering and trapping. Motivated by this, this study introduces wavy undulations for the proposed HTB to enhance the K_R and reduce the wave runup coefficient. The wave reflection K_R, wave runup K_H, horizontal force on PRS X_W, and vertical force on TWB Y_P by four structural configurations—seabed undulations: 1) upwave of the TWB with a trapping chamber, 2) seabed undulations upwave of TWB without trapping chamber, 3) seabed undulations underneath the TWB with a trapping chamber, and 4) seabed undulations underneath TWB without a trapping chamber—are evaluated against the relative wave frequency k_0h. Some physical properties of the TWB and seabed, such as the number of ripples in the TWB (five peaks and troughs, as shown in Figure 1), the undulation spacing length (S/B = 1), and the wavy surface amplitude (0.4), remain unchanged throughout the evaluation to facilitate numerical analysis.

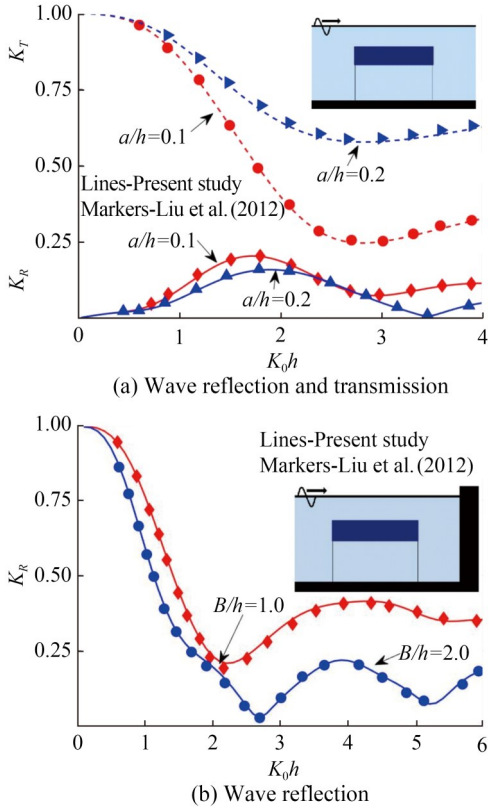

Figure 4 Verification of this study's numerical results with those reported by Liu et al. (2012)

4.2 Sloping seabed upwave of the TWB

Seabed undulations are the most common coastal process resulting from dynamic wave action. Sand erosion and accretion cause seabed undulations, and most previous studies approximated these undulations as multiple rigid steps (Behera et al., 2015; Venkateswarlu and Karmakar, 2020) to simplify mathematical formulations and solutions. In reality, the seabed is slopped, and this study examines a sloping seabed upwave of the thick wave plate placed far from the PRS.

4.2.1 Effect of wall porosity

The hydrodynamic performance of TWB with PRS is evaluated in the presence of an undulated seabed upwave of the barrier and an undulated seabed underneath the barrier. The back wall is partially reflective, meaning it reflects some wave energy while dissipating the rest. Technically, the PRS completely reflects wave energy when the property of C_R approaches unity (C_R = 1), and the wall is transparent to incident waves when C_R attains zero value (C_R = 0). Figure 5 presents the K_R, K_H, X_W, and Y_P versus k_0h for various values of wall reflection when B/h = 1, L/h = 1, a/h = 0.15, D/h = 0.2, θ = 30°, α = 0, and μ = 0.2. The K_R of the breakwater system aligns with the PRB reflection property for the initial values of relative water depth. The K_R pattern is oscillatory, consisting of multiple harmonic peaks and troughs. A linear decrease in K_R is observed across all wall reflection combinations as the relative water depth increases, which results from the reduction in wavelength. A pair of zero minima in K_R is observed at relative water depths of k_0h = 1.6 and k_0h = 3 for most of the input values of wall reflection C_R. This is attributed to standing wave formation in the chamber region owing to multiple interactions between incident waves and trapped wave energy. The K_R of the breakwater system is minimal when C_R = 0.2.

The primary peak in the K_H is observed near k_0h = 0.5, disappearing as wall reflection reduces owing to increased wave damping. A linear reduction in K_H is observed for all input values of wall reflection, with variations in wall reflection evident for longer wavelength waves. The effect of wall reflection on trapping and force coefficients is minimal as the wavelength reduces. A monotonic decrease in X_W is observed against the relative water depth for all wall reflection combinations. This trend is evident at the starting values of relative water depth, with X_W predictions becoming nearly identical as k_0h approaches k_0h = 2. The vertical force on the barrier Y_P is highly oscillatory against the relative water depth. A major peak for waves of higher wavelength and a minor peak for waves of moderate wavelength are observed across all wall reflection combinations. The predicted force on the barrier is maximum for higher wall reflection values and gradually decreases as wall reflection increases, owing to changes in wave damping.

4.2.2 Effect of chamber spacing

Figure 6 shows the K_R, K_H, X_W, and Y_P versus k_0h for various values of chamber spacing L/h when B/h = 1, a/h = 0.15, C_R = 1, D/h = 0.1, θ = 30°, α = 0, and μ = 0.2. The chamber spacing L/h = 0 indicates that the TWB is placed close to the PRS. The wave trapping and force coefficients

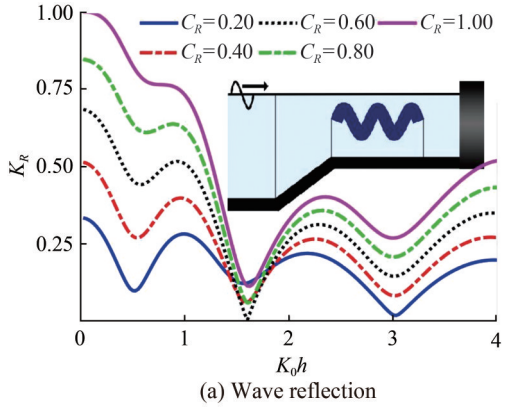

(a) Wave reflection

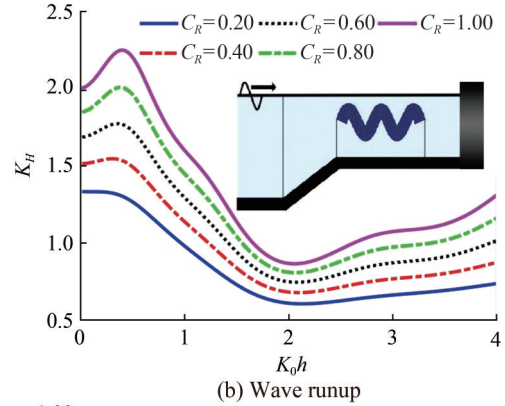

(b) Wave runup

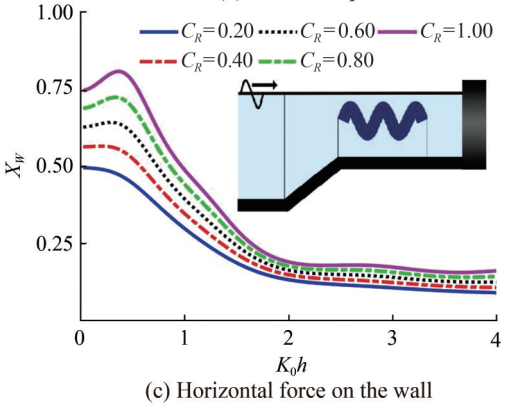

(c) Horizontal force on the wall

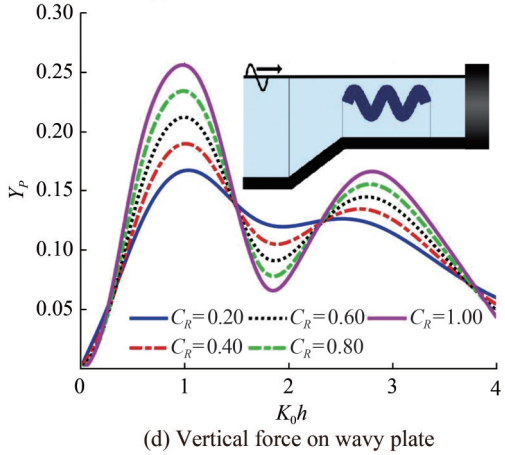

(d) Vertical force on wavy plate

Figure 5 Effect of wall porosity on K_R, K_H, X_W, and Y_P versus k_0h when $B/h = 1$, $L/h = 1$, $a/h = 0.15$, $D/h = 0.2$, $\theta = 30^o$, $\alpha = 0$, and $\mu = 0.2$

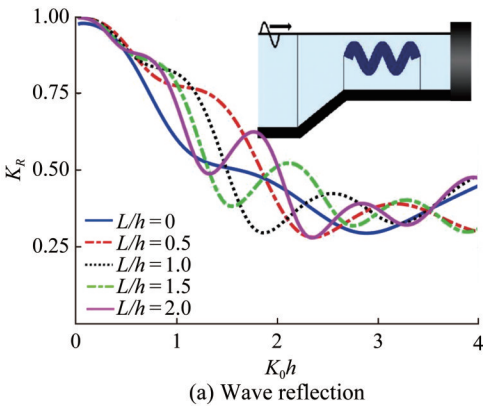

(a) Wave reflection

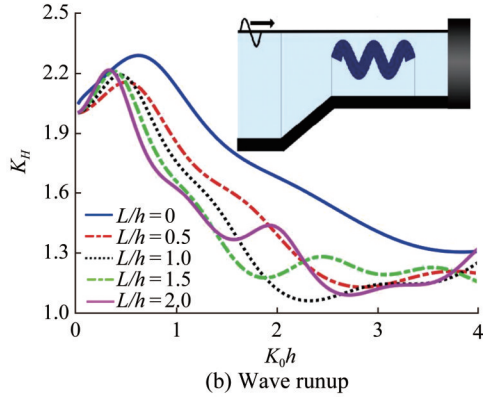

(b) Wave runup

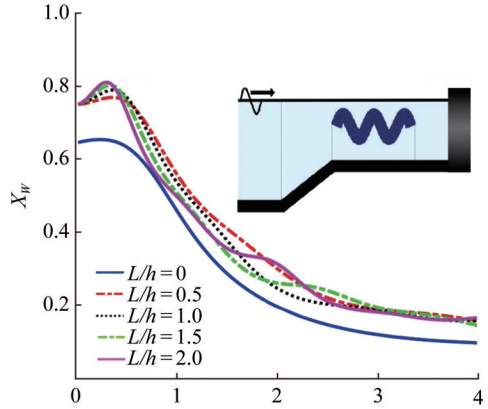

(c) Horizontal force on the wall

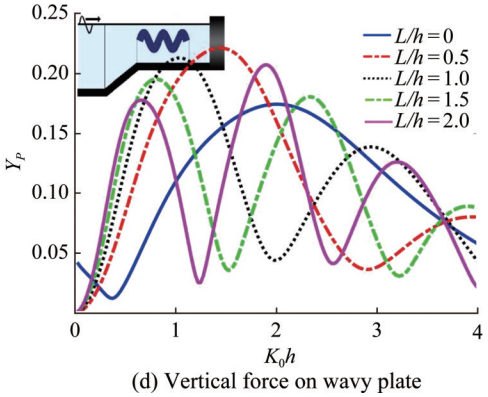

(d) Vertical force on wavy plate

Figure 6 Effect of chamber spacing on K_R, K_H, X_W, and Y_P versus k_0h when $B/h = 1$, $a/h = 0.15$, $C_R = 1$, $D/h = 0.1$, $\theta = 30^o$, $\alpha = 0$, and $\mu = 0.2$

are reported when the wall reflection is full $C_R = 1$. Thus, the full reflection $K_R = 1$ is observed for starting values of relative water depth. A nonoscillatory, monotonic reduction pattern of K_R by the breakwater system is observed against the relative water depth k_0h when the water chamber is absent. After introducing the trapping chamber, K_R becomes slightly oscillatory, with the intensity of oscillations increasing as the chamber spacing increases. Most previous studies have reported that the free chamber between the porous plate and back wall enhances fluid oscillations, resulting in harmonic peaks and troughs. In most cases, zero minima are observed owing to standing waves, and a similar pattern of coefficients is obtained in this study. The estimation of K_H is increased when the water chamber is absent owing to changes in wave damping, and as the chamber spacing increases, K_H decreases in an oscillatory manner. The K_H is almost zero when relative water depth approaches k_0h =2 owing to wave damping by the TWB. The K_H is higher in the no-chamber case, resulting in a minimal fluid force on the wall. However, after introducing the chamber, the wall force coefficient slightly increased owing to trapped wave energy. The force experienced by the TWB is minimal and attains a single peak when the chamber is absent. After introducing the chamber, the barrier experiences fluid force in an oscillatory manner, with an increase in the chamber spacing enhancing the oscillatory pattern in the form of harmonic peaks and troughs. However, the corresponding bandwidth decreases at higher spacing compared to lower spacing in the vertical force coefficient.

4.2.3 Effect of plate porosity

Figure 7 shows the K_R, K_H, X_W, and Y_P versus k_0h for various input values of TWB porosity μ when B/h = 1, L/h = 1, a/h = 0.2, C_R = 1, D/h = 0.1, α = 0, and θ = 30°. The μ = 0 illustrates that the incident wave interacts with the impermeable TWB installed far from the rigid seawall. Full reflection is observed by the impermeable TWB when it is installed far from the rigid wall. After introducing porosity, the wavy plate creates an oscillatory nature in the chamber owing to the chamber in the wave damping. A harmonic trough is observed for 10% porosity, which is the minimum compared to other input values of plate porosity. Similarly, the runup by the impermeable TWB is increased compared to other plate porosity combinations. The introduction of porosity minimizes K_H for waves of moderate to lower wavelengths. However, the impermeable TWB shows an oscillatory nature, with a global minimum of K_H observed as k_0h approaches k_0h = 1.8. The pattern of X_W is completely different when the impermeable TWB is installed. After introducing porosity, its effect on X_W remains minimal for input values. The estimation of Y_P exceeds expectations when the impermeable TWB is installed owing to zero wave damping. After introducing porosity, a double-peak pattern appears in the vertical force

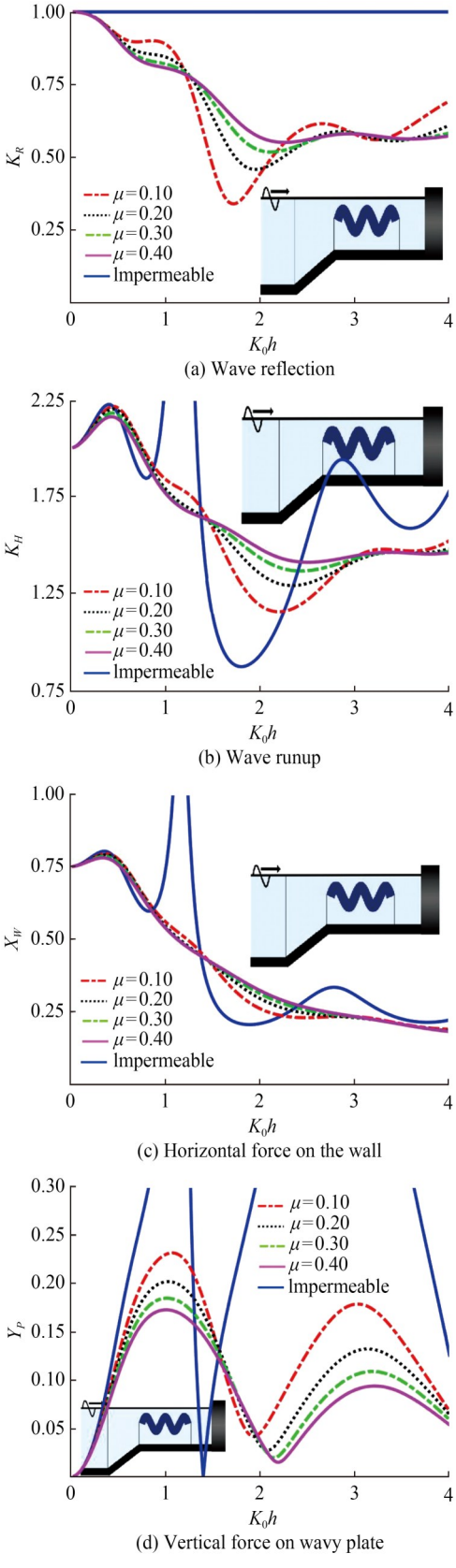

Figure 7 Effect of plate porosity on K_R, K_H, X_W, and Y_P versus k_0h when $B/h = 1$, $L/h = 1$, $a/h = 0.2$, $C_R = 1$, $D/h = 0.1$, $\alpha = 0$, and $\theta = 30°$

coefficient. The primary and secondary peaks in Y_P are observed at $k_0h = 1$ and $k_0h = 3$, respectively, for all input values of wavy plate porosity. The estimation of force is higher for lower porosity and lower for higher porosity owing to wave-induced flow through the available pore spaces of the medium. This explains the higher and lower wave damping by permeable thick or thin breakwaters against incident waves.

4.2.4 Effect of plate thickness

Figure 8 displays the K_R, K_H, X_W, and Y_P versus k_0h for various input values of TWB thickness D/h when $B/h = 1$, $L/h = 2$, $a/h = 0.1$, $C_R = 1$, $\mu = 0.2$, $\alpha = 0$, and $\theta = 30^o$. The magnitude of K_R is higher when the plate thickness is minimal. However, as the plate thickness increases, the minimal K_R—and occasionally global minima—is observed for waves with moderate to minimal wavelengths. The increase in plate thickness accelerates the oscillatory nature of trapping coefficients, possibly attributed to changes in wave damping. The runup also reduces as the plate thickness increases, and the plate thickness does not affect the trapping coefficient from $D/h = 0.15$ to $D/h = 0.25$. The wall experiences a maximum fluid force when the plate thickness is minimum, while the wavy barrier experiences a maximum fluid force when the plate thickness is maximum. Thus, the study suggests a moderate plate thickness $D/h = 0.15$ to achieve well-balanced trapping and force coefficients for further research and application of thick plates.

4.2.5 Effect of bottom undulation

Figure 9 shows the K_R, K_H, X_W, and Y_P versus k_0h for various seabed profiles α when $B/h = 3$, $L/h = 2$, $a/h = 0.2$, $D/h = 0.2$, $\theta = 30^o$, and $\mu = 0.2$. Various kinds of seabed undulations, including sloppy ($\alpha = 0$), protrusion type-A ($\alpha = 1$), protrusion type-B ($\alpha = 2$), concave seabed ($\alpha = -1$), and depression ($\alpha = -2$), are proposed, with their impact on the variation of wave trapping and force coefficients against relative water depth k_0h evaluated. The trends of trapping and force coefficients are similar for all the proposed seabed configurations. However, the variation of coefficients at each peak and trough is notable, and thus zoomed views are provided. The sloppy seabed performs minimal variation at each peak compared to all other seabed profiles in the reflection coefficients. Very minimal variation is observed in the K_H, X_W, and the vertical force of the TWB owing to changes in seabed profiles.

4.3 Effect of wall porosity in the absence of a chamber

4.3.1 Effect of wall reflection

In general, trapping chambers cause fluid oscillations inside the chamber as the trapped wave energy available between the permeable and nonpermeable walls tends to

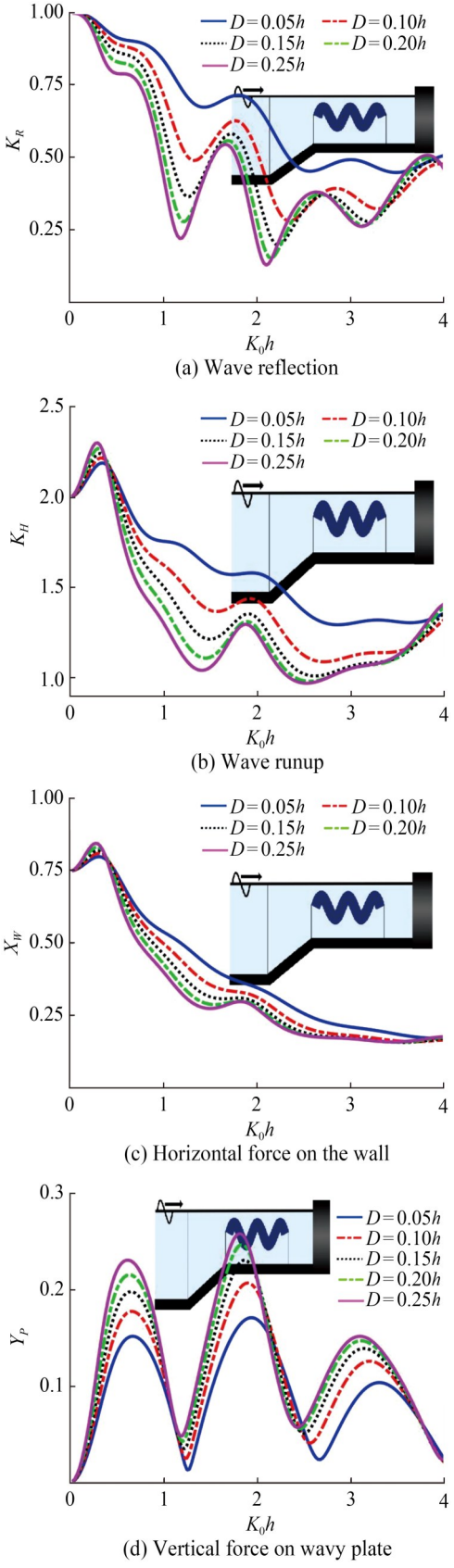

Figure 8 Effect of plate thickness on K_R, K_H, X_W, and Y_P versus k_0h when $B/h = 1$, $L/h = 2$, $a/h = 0.15$, $C_R = 1$, $\mu = 0.2$, $\alpha = 0$, and $\theta = 30^o$

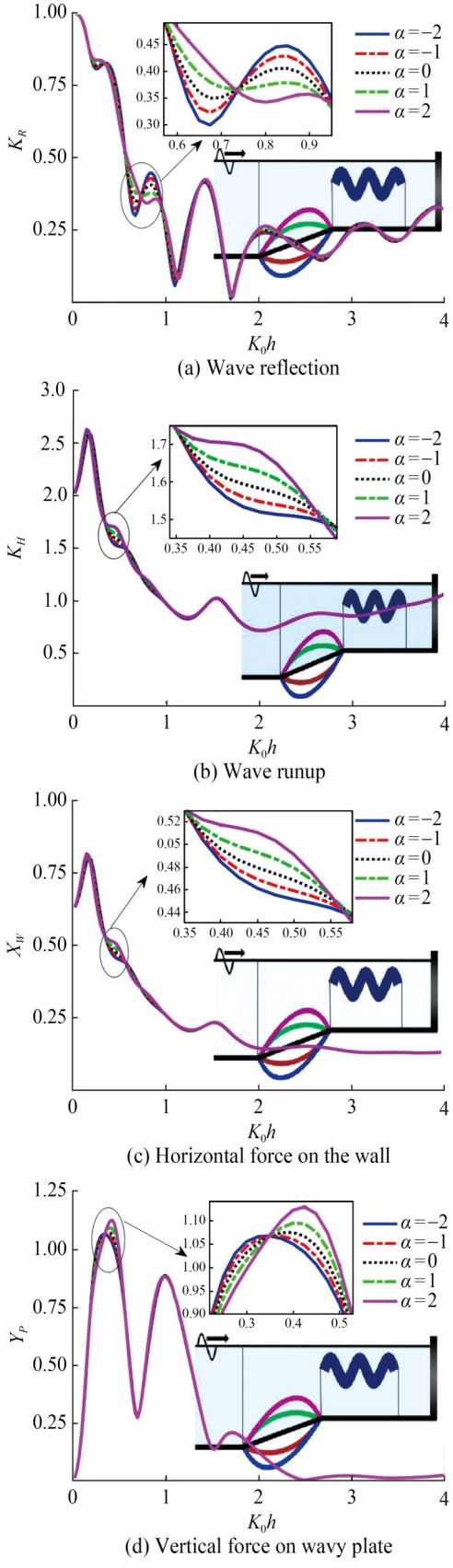

Figure 9 Effect of bottom undulation on K_R, K_H, X_W, and Y_P versus k_0h when $B/h = 3$, $L/h = 2$, $a/h = 0.2$, $D/h = 0.2$, $\theta = 30^o$, and $\mu = 0.2$

oscillate owing to the back-and-forth motion of the incident waves. Thus, this study attempted to evaluate the effect of wall reflection on variations in wave trapping and force coefficients. Figure 10 illustrates the K_R, K_H, X_W, and Y_P versus k_0h for various input values of wall reflection C_R when $B/h = 1$, $L/h = 0$, $a/h = 0.15$, $C_R = 1$, $D/h = 0.1$, $\theta = 30^o$, $\alpha = 0$, and $\mu = 0.2$. The effect of wall reflection on trapping and force coefficients is reported as a function of relative water depth. The K_R by breakwater is slightly oscillatory, with the magnitude of oscillations being minimal for the breakwater without a chamber compared to the breakwater with a water chamber. A decreasing pattern is observed in the K_R for all the combinations of wall reflection, and the estimation of K_R is high when the wall reflection is high. A zero minimum is observed for $C_R = 0.2$ when $k_0h = 2.8$. A decreasing pattern is observed in the K_H, with the maximum value occurring when wall reflection is highest owing to zero wave damping. As wall reflection decreases, the minimal K_H by the breakwater is observed because of an increase in wave damping. The pattern of wall force aligns with K_H, and the effect of wall porosity is notable when k_0h is varied within the range $0.1 \leqslant k_0h \leqslant 2$. Beyond this range, the effect of wall reflection becomes negligible. In the presence of a water chamber, a double-peak pattern of vertical force (Figure 5(d)) is observed, whereas in its absence, Y_P with a single peak is observed against the relative water depth. The effect of wall reflection is higher at the point of global optima $k_0h = 2$, and zero minima are observed at $k_0h = 0.4$ for $C_R = 0.8$. The wavy barrier experiences the greatest fluid force when $C_R = 1$, near $k_0h = 2$.

4.3.2 Effect of bottom undulation

Figure 11 shows K_R, K_H, X_W, and Y_P versus k_0h for various seabed profiles α when $B/h = 3$, $L/h = 0$, $a/h = 0.2$, $D/h = 0.2$, $\theta = 30^o$, and $\mu = 0.2$. The variation in trapping and force coefficients is evident in the absence of a trapping chamber compared to in the presence of a trapping chamber (Figure 9). The K_R is almost identical for all combinations of seabed profiles. However, the K_H is minimal by TWB after introducing the protrusion type-B ($\alpha = 2$) seabed, which may be attributed to the amplification of wave energy. Therefore, the corresponding force coefficients are maximum for the protrusion type-B ($\alpha = 2$) seabed compared to other seabed profiles. Hence, this study recommends using sloppy seabeds instead of protrusion type B owing to minimal forces on the TWB.

4.4 Sloping seabed underneath the TWB

The change in seabed profiles is a common phenomenon considered by several authors when evaluating various types of breakwaters. In some coastal areas, floating structures are installed away from the undulated seabed, while in other locations, floating structures are placed on the undu-

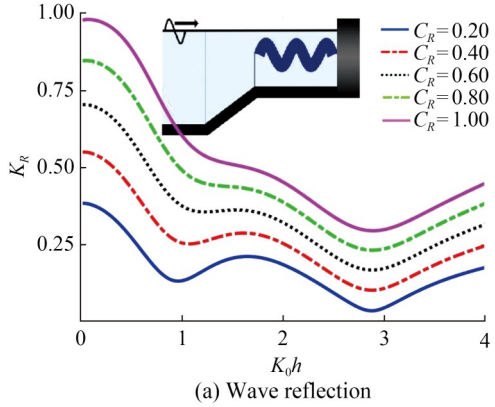

(a) Wave reflection

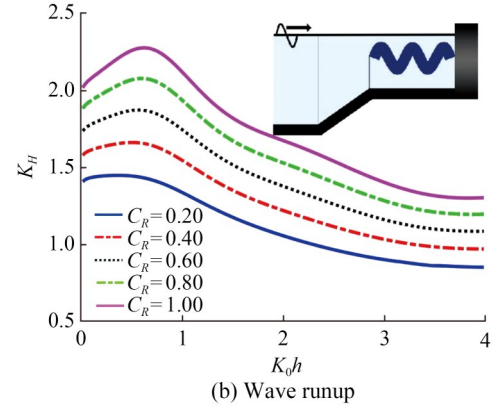

(b) Wave runup

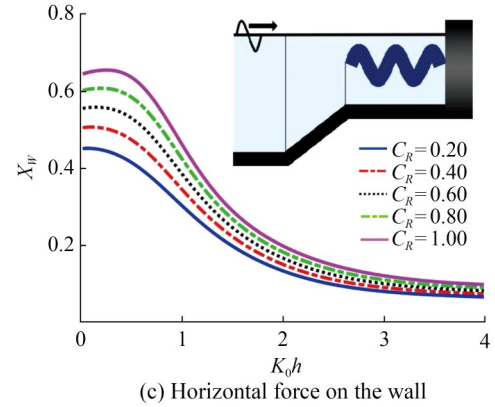

(c) Horizontal force on the wall

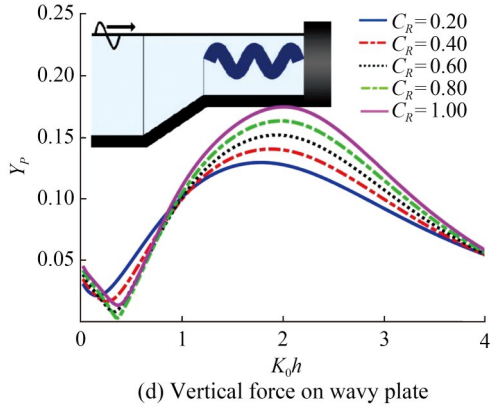

(d) Vertical force on wavy plate

Figure 10 Effect of wall porosity on K_R, K_H, X_W, and Y_P versus k_0h when $B/h = 1$, $L/h = 0$, $a/h = 0.15$, $C_R = 1$, $D/h = 0.1$, $\theta = 30^o$, $\alpha = 0$, and $\mu = 0.2$

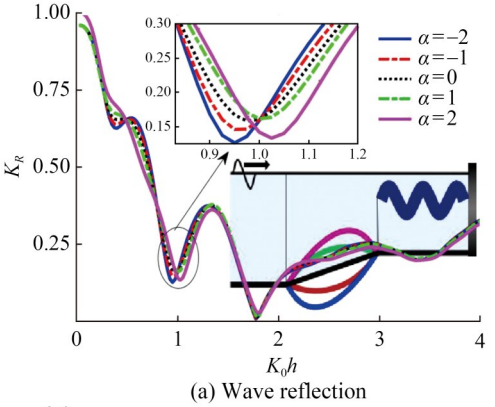

(a) Wave reflection

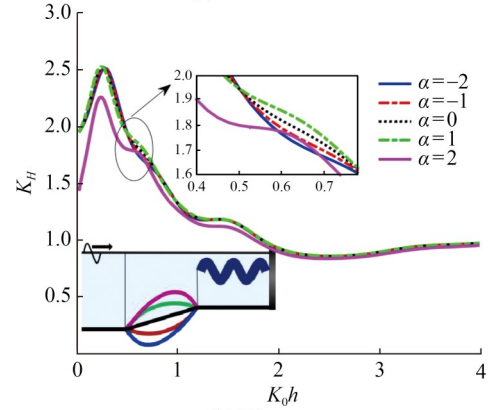

(b) Wave runup

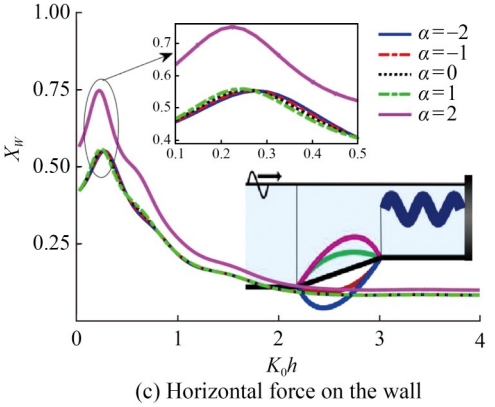

(c) Horizontal force on the wall

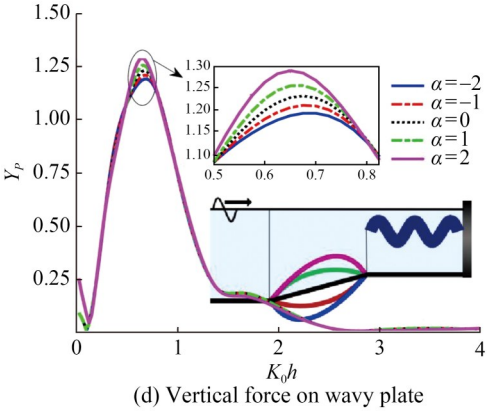

(d) Vertical force on wavy plate

Figure 11 Effect of bottom undulation on K_R, K_H, X_W, and Y_P versus k_0h when $B/h = 3$, $L/h = 0$, $a/h = 0.2$, $D/h = 0.2$, $\theta = 30^o$, and $\mu = 0.2$

lated seabed where space is limited. Thus, the installation of the TWB is classified into i) undulated seabed upwave of the TWB and ii) undulated seabed underneath the TWB to evaluate its impact on wave trapping. In this subsection, the TWB is installed on the undulated seabed, with two different conditions, including i) TWB with chamber and ii) without chamber, examined for various input values of TWB properties and seabed geometries.

4.4.1 Effect of wall porosity

Figure 12 illustrates K_R, K_H, X_W, and Y_P versus k_0h for various input values of wall reflection C_R when $B/h = 1$, $L/h = 1$, $a/h = 0.15$, $D/h = 0.1$, $\theta = 30°$, $\alpha = 0$, and $\mu = 0.2$. The value of C_R is varied with $0.2 \leqslant C_R \leqslant 1$, where $C_R = 1$ indicates the total energy reflection and $C_R = 0$ corresponds to a fully transparent wall that transmits all incident wave energy. The pattern of all trapping and force coefficients closely follows that of Figure 5 (sloping seabed away from wavy barrier) and Figure 10 (sloping seabed away from wavy barrier with no chamber). After rearranging the location of the sloping seabed, the magnitude of oscillations is minimal compared to a sloping seabed away from the TWB and maximum compared to a sloping seabed away from the TWB without a chamber. The variation in trapping and force coefficients is evident at each harmonic peak and trough compared to other structural configurations. The magnitude of oscillations is noticeable when the back wall is impermeable, and a substantial reduction in coefficients is observed after reducing wall reflection.

4.4.2 Effect of wavy plate depth

The depth of the TWB is crucial in wave scattering and trapping analysis against incident waves. The hydrodynamic coefficients change rapidly based on the depth of the submergence of the TWB. Thus, the variation of hydrodynamic coefficients is examined for changes in wavy barrier depth when located upon the sloping seabed. Figure 13 shows the K_R, K_H, X_W, and Y_P versus k_0h for various input values of wavy barrier submergence depth when $B/h = 1$, $L/h = 1$, $C_R = 1$, $D/h = 0.1$, $\theta = 30°$, $\alpha = 0$, and $\mu = 0.2$. A sharp drop in K_R, followed by zero minima, is observed when the plate is installed near the mean free water level ($a/h = 0.15$) relative to k_0h. This results from the increased wave action near the wavy plate, which causes notable wave damping. The global minimum of K_R for $a/h = 0.15$ results from standing wave formation owing to the interaction between reflected and incident waves in the wave trapping zone. After increasing the submergence depth, a moderate increase in K_R is observed for k_0h varied within $1.8 \leqslant k_0h \leqslant 4$, which is owing to the minimal participation of the TWB in reducing K_R and increasing wave damping. The role of the wavy barrier in dissipating wave energy is negligible for submergence depth varied within $0.3 \leqslant a/h \leqslant 0.35$, with the back wall playing a predominant role in attenuating the wave energy in this scenario. Minimal K_H is obtained for sub-

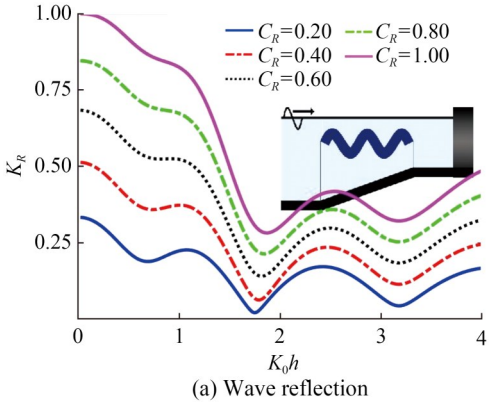

(a) Wave reflection

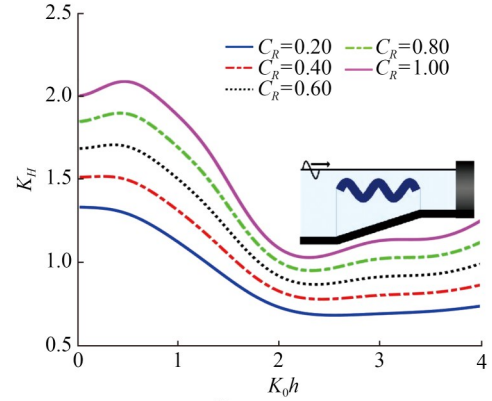

(b) Wave runup

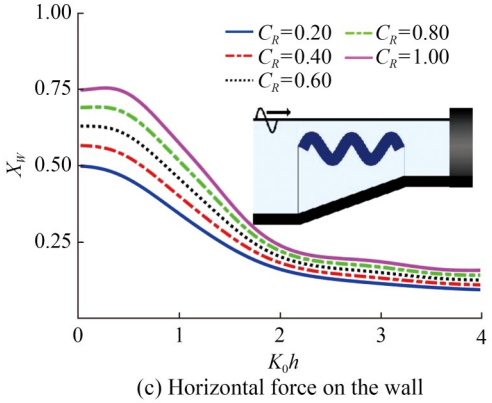

(c) Horizontal force on the wall

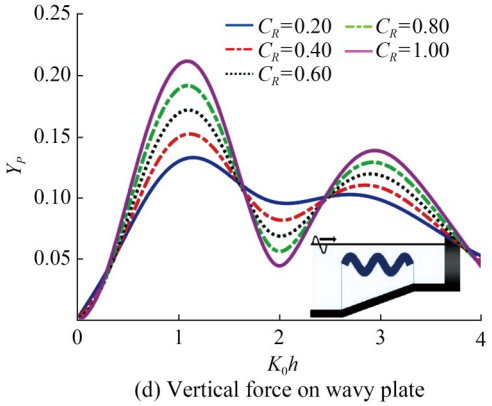

(d) Vertical force on wavy plate

Figure 12 Effect of wall porosity on K_R, K_H, X_W, and Y_P versus k_0h when $B/h = 1$, $L/h = 1$, $a/h = 0.15$, $D/h = 0.1$, $\theta = 30°$, $\alpha = 0$, and $\mu = 0.2$

mergence depth $a/h = 0.15$ as the wavy barrier is installed near the free surface, which causes higher wave damping and wave trapping. After increasing the submergence depth, a moderate K_H is observed for $a/h = 0.25$ and higher K_H for submergence depth varied within $0.3 \leqslant a/h \leqslant 0.35$ owing to the minimal participation of the wavy barrier in trapping and dissipating the incident waves. The PRS experiences maximal fluid force for starting values of k_0h, which decreases linearly as the relative water depth k_0h increases. The role of wavy barrier submergence depth is notable when installed near the free surface but becomes negligible at greater submergence depths. The double-peak pattern is observed in the X_W against the relative water depth. The effect of submergence depth is greatest at the primary peak, and an almost zero minimum of X_W is predicted by the numerical model when the relative water depth approaches $k_0h = 2.2$. The variation of X_W is high near the second peak for different values of submergence depth owing to the reduction in wavelength. The TWB attenuates waves of minimal length when installed near the free surface and experiences increased fluid force. Thus, the submergence depth of $a/h = 0.15$ is suitable for attenuating waves of higher and moderate wavelengths.

4.4.3 Effect of wavy plate porosity

The study evaluates the effect of TWB porosity when installed on a sloping seabed far from the wall. Figure 14 shows the K_R, K_H, X_W, and Y_P versus k_0h for various input values of wavy barrier porosity when $B/h = 1$, $L/h = 1$, $a/h = 0.15$, $C_R = 1$, $D/h = 0.15$, $\alpha = 0$, and $\theta = 30^\circ$. The full K_R is observed when the TWB is impermeable and installed on a sloppy seabed, with the effect of k_0h being negligible. After introducing porosity, the TWB initiates the oscillatory pattern in the form of harmonic peaks and troughs. The zero minima of K_R is observed at $\mu = 0.1$ for $k_0h = 1.45$ owing to standing wave formation from the reinteraction of reflected and incident waves. Thereafter, K_R demonstrates a linear increase with harmonic oscillations for $\mu = 0.1$. The magnitude of harmonic oscillations is reduced after increasing the porous TWB. The $\mu = 0.4$ and $\mu = 0.5$ show almost identical estimations of K_R against k_0h varied within $2 \leqslant k_0h \leqslant 4$, which results from the saturation stage of dissipation attained by TWB.

The K_H is maximum when the wavy barrier is impermeable. After introducing porosity, nearly identical K_H values are observed for all input values of TWB porosity, indicating that the TWB plays a minimal role in attenuating the K_H for k_0h varied within $2.5 \leqslant k_0h \leqslant 4$. The wall experiences maximum fluid force when the TWB is impermeable. After introducing porosity, X_W follows a linear reduction pattern with negligible variations. A double-peak oscillatory pattern is observed in Y_P when the barrier is permeable. Similarly, Y_P approaches ultrahigh values when the TWB is impermeable. Its variation is evident at the major peak for all input values of barrier porosity, with a similar pattern

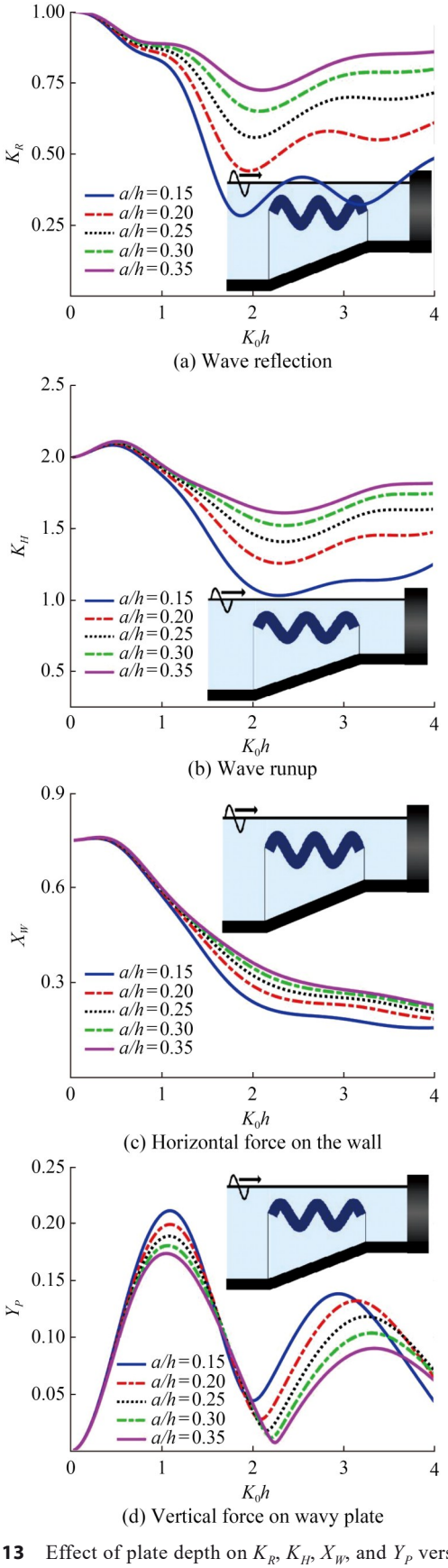

Figure 13 Effect of plate depth on K_R, K_H, X_W, and Y_P versus k_0h when $B/h = 1$, $L/h = 1$, $C_R = 1$, $D/h = 0.1$, $\theta = 30^\circ$, $\alpha = 0$, and $\mu = 0.2$

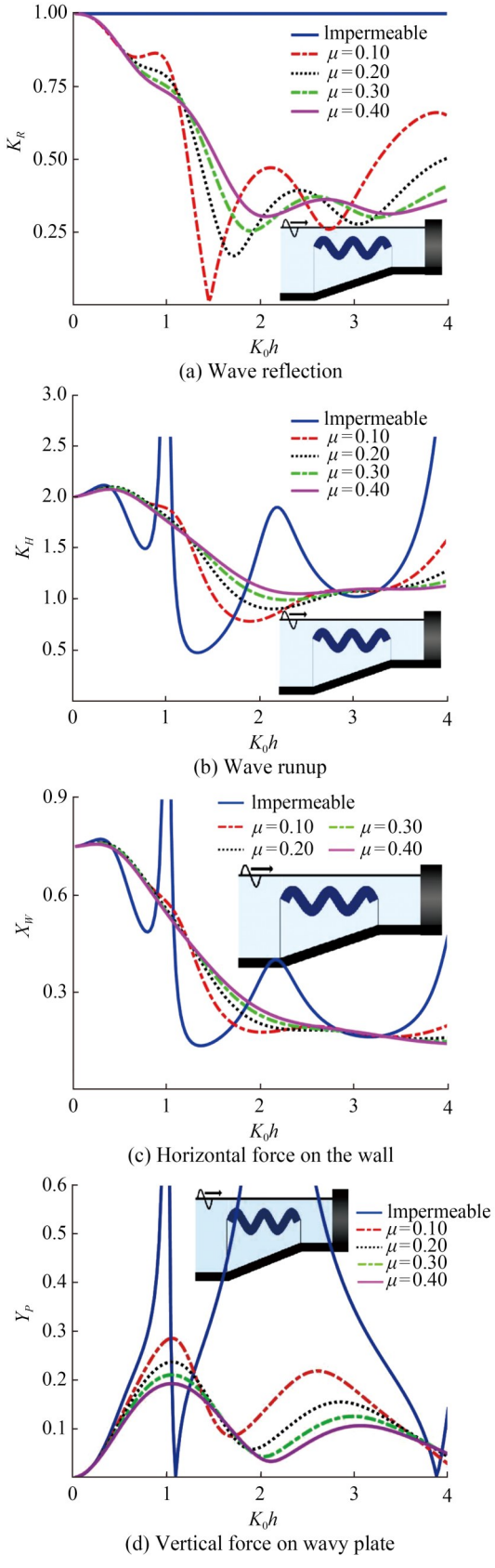

Figure 14 Effect of plate porosity on K_R, K_H, X_W, and Y_P versus k_0h when $B/h = 1$, $L/h = 1$, $a/h = 0.15$, $C_R = 1$, $D/h = 0.15$, $\alpha = 0$, and $\theta = 30^o$

observed at the secondary peak. The porosity effect is noticeable near the secondary peak compared to the major peak near $k_0h = 1$. Thus, this study suggests the TWB porosity within $0.1 \leqslant \mu \leqslant 0.2$ to balance the wave trapping and force coefficients when the sloping seabed is beneath.

4.4.4 Effect of plate thickness

Figure 15 shows the K_R, K_H, X_W, and Y_P against k_0h for various input values of wave plate thickness D/h when $B/h = 1$, $L/h = 2$, $a/h = 0.1$, $C_R = 1$, $\mu = 0.2$, $\alpha = 0$, and $\theta = 30^o$. The trapping and force coefficient patterns are nearly identical to those in Figure 8 (TWB near sloping seabed with wall). The variation of coefficients is noticeable at each harmonic peak and trough. Enhanced harmonic peaks are observed for the sloppy seabed away from the TWB, and they may be observed clearly for Y_P near each harmonic peak and trough.

4.4.5 Effect of chamber spacing

The effect of chamber spacing on wave trapping and force coefficients is reported when the wavy plate is installed over the sloping seabed. Figure 16 shows the K_R, K_H, X_W, and Y_P versus k_0h for various input values of chamber spacing when $B/h = 1$, $a/h = 0.1$, $C_R = 1$, $D/h = 0.2$, $\theta = 30^o$, $\alpha = 0$, and $\mu = 0.2$. The chamber spacing $L/h = 0$ indicates that the wavy plate is installed near the back wall, with the sloping seabed beneath the TWB. A linear decline in K_R is observed for all L/h combinations, with a zero minima observed at K_R when k_0h approaches $k_0h = 1.2$ possibly attributed to the formation of standing waves. After attaining a minimum value, K_R increases and attains an identical value with a slightly upward trend for all L/h combinations. The effect of L/h is evident in the K_R against k_0h varied within $0.5 \leqslant k_0h \leqslant 1.5$. A higher K_H is observed for the no-chamber case, and after introducing a finite chamber, a slight reduction in K_H is observed for all the input values of chamber spacing. The increase in relative water depth k_0h reduces K_H when varied within $0.1 \leqslant k_0h \leqslant 2$, after which the chamber spacing becomes negligible on K_H coefficient. The vertical wall experiences minimal fluid force when the chamber is absent. After introducing the chamber between the TWB and the vertical wall, a slight increase in the X_W is observed, with the effect of chamber spacing being negligible. A single peak is observed in X_W against k_0h for specific values of chamber spacing L/h varied within $0 \leqslant L/h \leqslant 1.0$, and a pair of peaks are observed when L/h is varied within $1.5 \leqslant L/h \leqslant 2$. The barrier experiences the greatest fluid force when the chamber spacing approaches $L/h = 1$ and $k_0h = 1$. Overall, moderate chamber spacing is suitable for distributing wave trapping and force coefficients effectively.

4.4.6 Effect of bottom undulation

Figure 17 illustrates the K_R, K_H, X_W, and Y_P versus k_0h for various seabed profiles α when $B/h = 3$, $L/h = 2$, $a/h = 0.15$, $D/h = 0.2$, $\theta = 30^o$, and $\mu = 0.2$. Various types of sea-

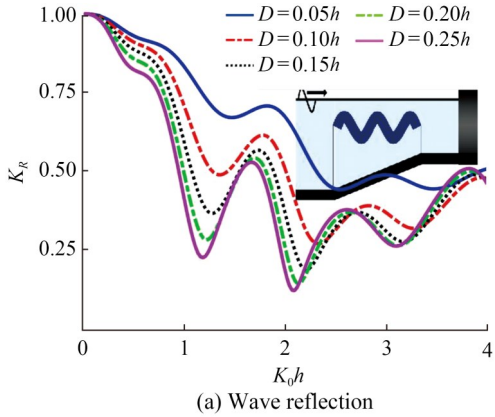

(a) Wave reflection

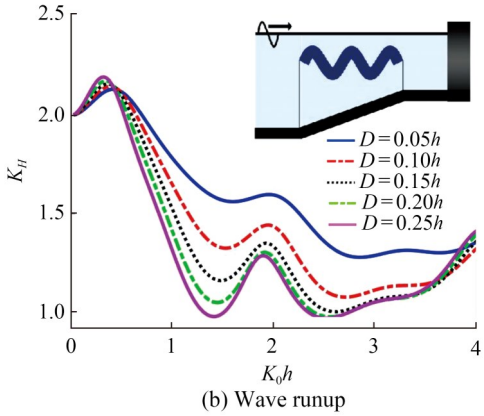

(b) Wave runup

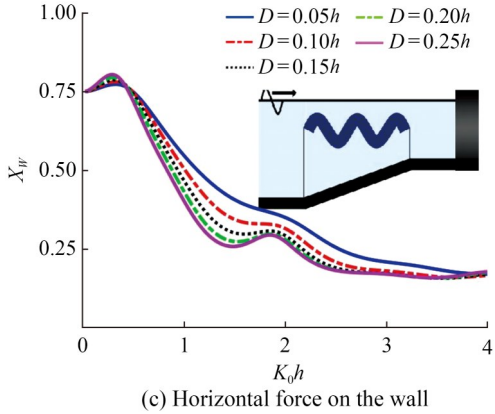

(c) Horizontal force on the wall

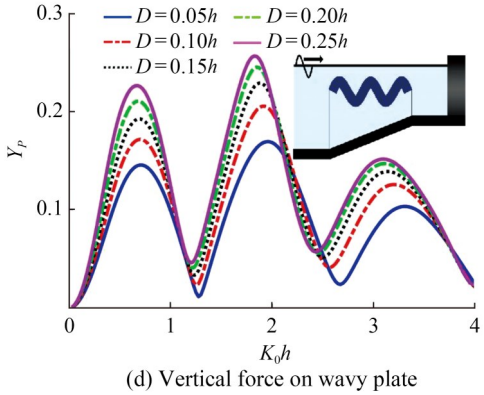

(d) Vertical force on wavy plate

Figure 15 Effect of plate porosity on K_R, K_H, X_W, and Y_P versus k_0h when $B/h = 1$, $L/h = 2$, $a/h = 0.15$, $C_R = 1$, $\theta = 30°$, $\alpha = 0$, and $\mu = 0.2$

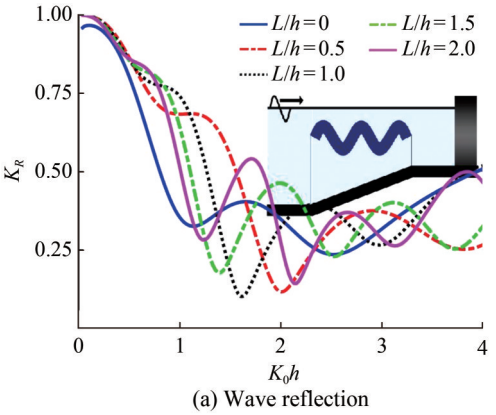

(a) Wave reflection

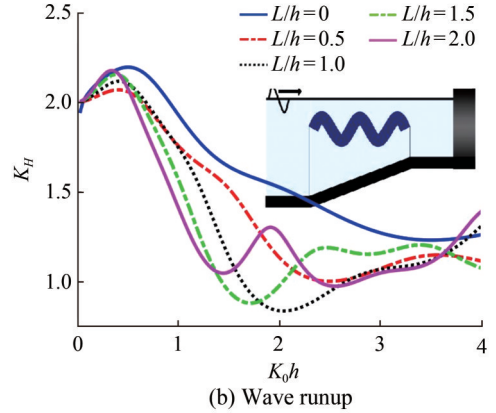

(b) Wave runup

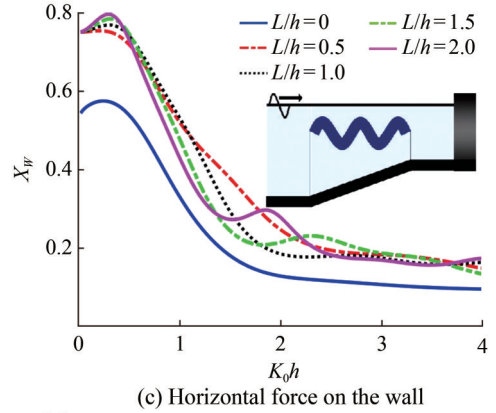

(c) Horizontal force on the wall

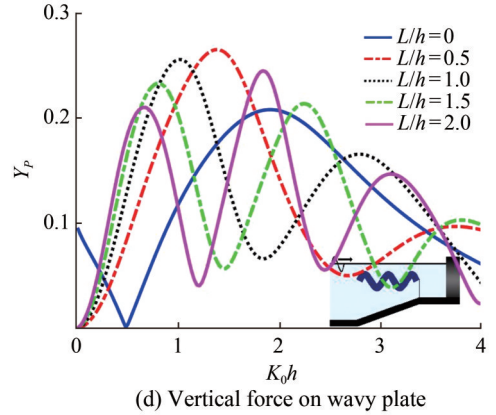

(d) Vertical force on wavy plate

Figure 16 Effect of chamber spacing on K_R, K_H, X_W, and Y_P versus k_0h when $B/h = 1$, $a/h = 0.15$, $C_R = 1$, $D/h = 0.2$, $\theta = 30°$, $\alpha = 0$, and $\mu = 0.2$

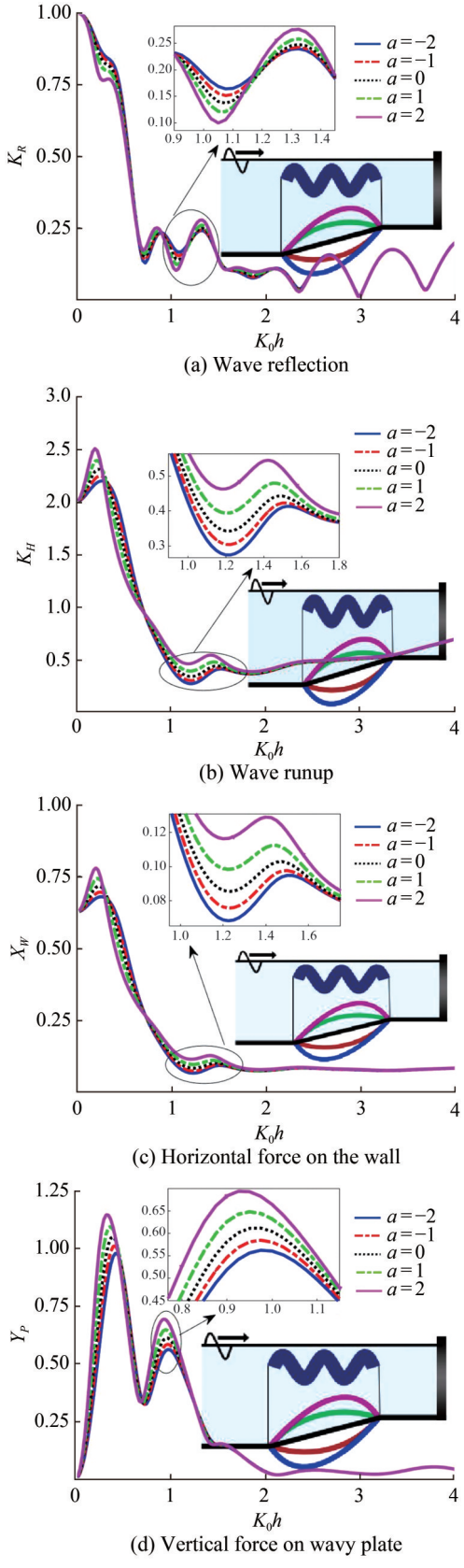

Figure 17 Effect of bottom undulation on K_R, K_H, X_W, and Y_P versus k_0h when $B/h = 3$, $L/h = 2$, $a/h = 0.15$, $D/h = 0.2$, $\theta = 30°$, and $\mu = 0.2$

bed undulations are introduced and evaluated when they are present underneath the TWB in the trapping chamber. The oscillatory phenomenon is observed, with the magnitude of oscillations being minimal in the present case compared to that in Figure 9. The location of the seabed undulation is evident as the oscillations in the wave trapping and force coefficients are minimized. This is because the waves propagate between the TWB and seabed undulations, which enhances fluid damping. Overall, protrusion type-B shows a slightly higher prediction of trapping and force coefficients than the other seabeds, and these conclusions align with those reported in the previous predictions (Figure 9). The sloppy seabed predicts moderate values of coefficients against k_0h, while depression-type seabed shows a minimum prediction of coefficients compared to all other seabed types when the TWB is installed over the seabed undulations with a trapping chamber.

4.5 Effect of plate porosity without a chamber

4.5.1 Effect of TWB porosity

In this condition, a wavy barrier is installed close to the vertical wall, with a sloping seabed beneath the TWB. The effect of plate porosity on the trapping and force coefficients against relative water depth is presented. Figure 18 shows the K_R, K_H, X_W, and Y_P versus k_0h for various input values of plate porosity when $B/h = 1$, $L/h = 0$, $a/h = 0.15$, $C_R = 1$, $D/h = 0.15$, $\alpha = 0$, and $\theta = 30°$. Full reflection is observed after installing the impermeable TWB owing to zero wave damping. After introducing porosity, a double trough reflection pattern is observed, with the secondary trough disappearing as porosity increases. However, the minimal K_R is observed for the plate porosity varied within $0.1 \leqslant \mu \leqslant 0.2$ in the absence of chamber spacing with a sloping seabed. The barrier reflects the maximum wave energy when it is impermeable, but K_H is maximum compared to other combinations. After introducing porosity, a decreasing trend is observed in the K_H coefficient, with minimal variation after increasing the plate porosity.

The wall experiences minimal fluid force as most of the wave energy is identified in K_H, indicating that most of the wave energy interacting with the rigid wall is reflected toward the seaside, while the remaining energy is considered as K_H. After introducing the porous barrier, high porosity results in increased force, while low porosity leads to reduced force. This occurs because of wave-induced flow through the thick plate. The barrier experiences maximum fluid when it is rigid, and after introducing porosity, a single peak pattern is observed. A higher fluid force is observed when plate porosity is minimal, and an increase in porosity reduces Y_P owing to increased particle motion through the barrier and wave damping. Therefore, this study suggests a plate porosity varying within $0.1 \leqslant \mu \leqslant 0.2$ to achieve well-balanced trapping and force coefficients.

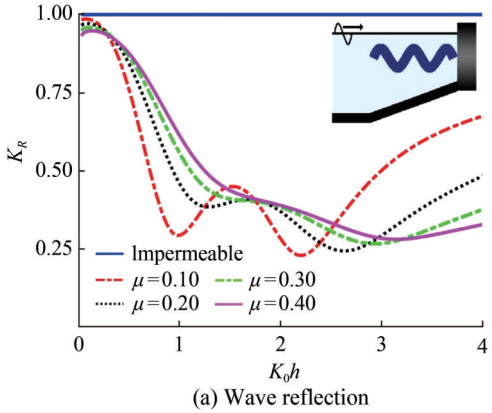

(a) Wave reflection

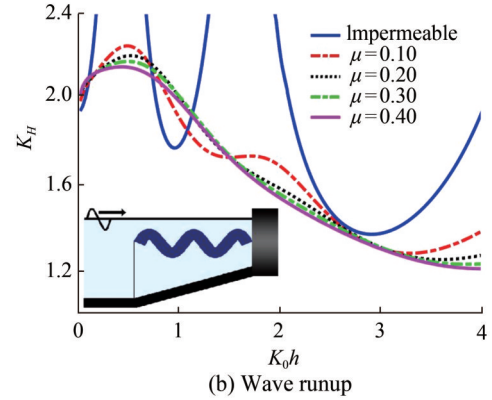

(b) Wave runup

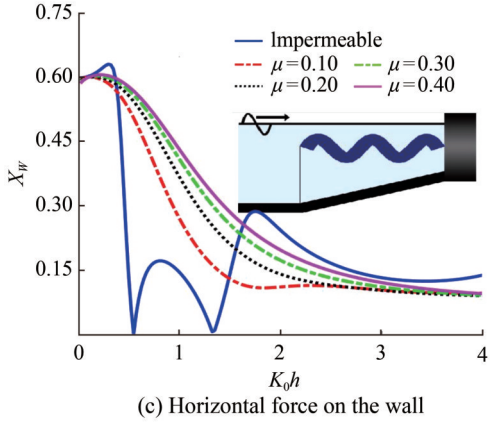

(c) Horizontal force on the wall

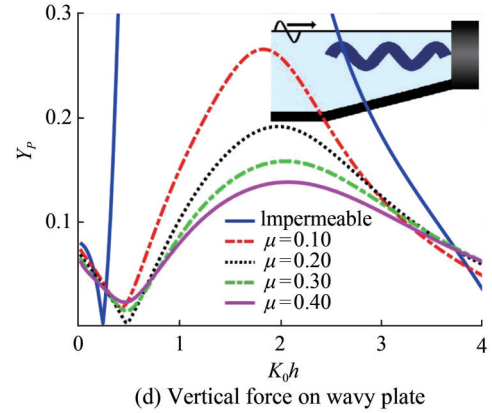

(d) Vertical force on wavy plate

Figure 18 Effect of plate porosity on K_R, K_H, X_W, and Y_P versus k_0h when B/h = 1, L/h = 0, a/h = 0.15, C_R = 1, D/h = 0.15, α = 0, and θ = 30°

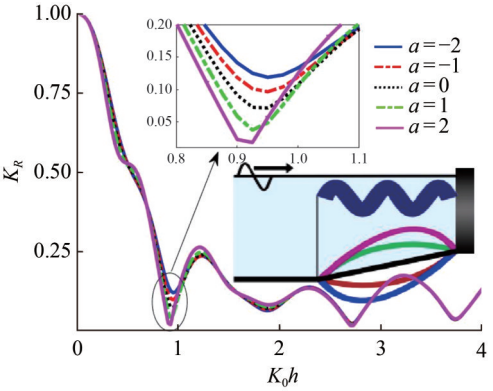

(a) Wave reflection

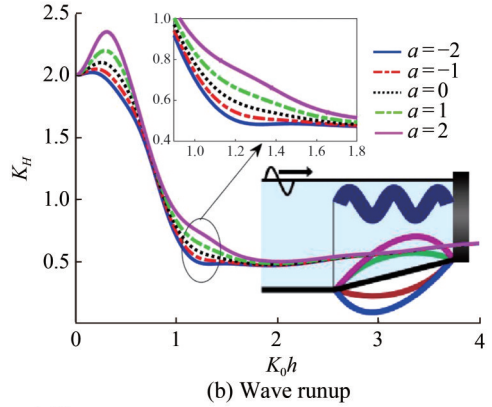

(b) Wave runup

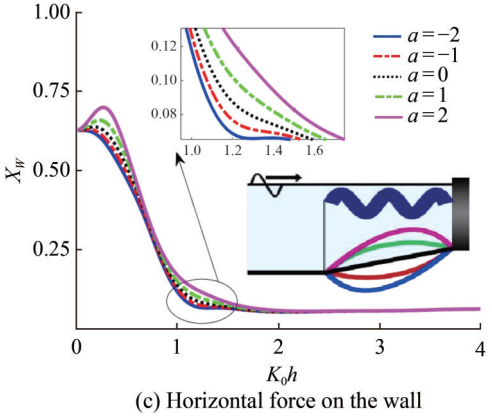

(c) Horizontal force on the wall

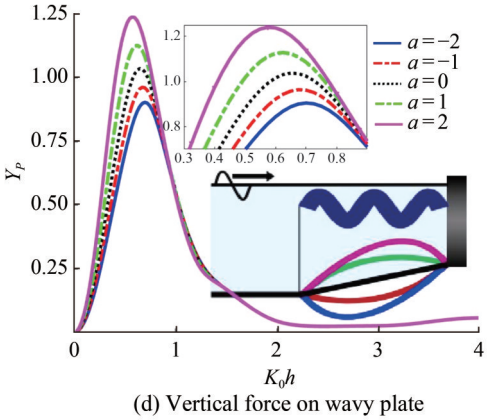

(d) Vertical force on wavy plate

Figure 19 Effect of bottom undulation on K_R, K_H, X_W, and Y_P versus k_0h when B/h = 3, L/h = 0, a/h = 0.15, D/h = 0.2, θ = 30°, and μ = 0.2

4.5.2 Effect of bottom undulation

Figure 19 demonstrates the K_R, K_H, X_W, and Y_P versus k_0h for various seabed profiles α when $B/h = 3$, $L/h = 0$, $a/h = 0.15$, $D/h = 0.2$, $\theta = 30^o$, and $\mu = 0.2$. The effects of various seabed undulations are introduced and evaluated when they are present underneath the TWB in the absence of the trapping chamber. The pattern of trapping coefficients closely matches that shown in Figure 17. The effect of seabed variation is minimal on the reflection, runup, and X_W. A single peak pattern is observed in Y_P, with the effect of seabed undulations evident near the optima. Higher Y_P is obtained by TWB when the seabed is of protrusion type-B ($\alpha = 2$), while minimal Y_P occurs with a depression-type seabed ($\alpha = -2$). Moderate coefficient values are achieved by TWB when the seabed has a sloppy nature.

5 Conclusions

This study examined the physical mechanism of wave trapping by a TWB when installed near a PRS. The sloping type of seabed undulation was included while analyzing the breakwater. The MBEM was employed to assess the effects of barrier porosity, wall reflection, chamber spacing, plate thickness, and barrier submergence depth against the relative water depth on wave trapping coefficients (reflection and runup) and force coefficients (vertical force on the barrier and horizontal force on the wall). The following conclusions are drawn from the numerical investigation:

1) A pair of zero minima in the wave reflection pattern is obtained against the relative water depth when $k_0h = 1.6$ and $k_0h = 3$, respectively, for maximum combinations of wall reflection C_R owing to the formation of standing waves. A moderate value of wall reflection $C_R = 0.5$ is recommended based on the numerical results.

2) For the TWB, a porosity range of $0.1 \leqslant \mu \leqslant 0.2$, thickness of $D/h = 0.1$, and submergence depth of $a/h = 0.15$ are suggested to achieve well-balanced trapping and force coefficients.

3) The undulated seabed away from the TWB enhanced the fluid resonance compared to other proposed combinations. Minimal wave reflection with a double-peak pattern is observed for the water chamber, and a single peak is observed for the no-water chamber in the presence of TWB.

4) When the impermeable TWB is installed against the incident waves, the global minima of wave runup occurs at $k_0h = 1.8$ in an oscillatory manner, and the impermeable TWB experiences a higher vertical force coefficient.

5) The TWB on the undulated seabed experiences the greatest fluid force when the chamber spacing approaches $L/h = 1$ for $k_0h = 1$. The sloppy seabed upwave of the TWB with a trapping chamber is recommended for balanced coefficients.

We affirm that the conclusions of this study are limited to the test conditions outlined in the figure captions. This study offers a solution for replacing partial structures without affecting hydrodynamic performance. Previous studies recommend gravity-type breakwaters for optimal protection against incident wave energy. However, installing gravity-type breakwaters is challenging when the seabed is undulating and sensitive. In locations with larger water depths, undulated bottom, and sensitive seabed, wavy structures are a better option than other types of floating and bottom-fixed breakwaters, such as submerged continuous breakwaters in Weihai City, pile-rock breakwaters along the Dongying Coast (China), and those in the Mekong Delta region. Under these conditions, the TWB can provide sufficient tranquil conditions against incident waves. This study employed linearized wave theory, which is a limitation and could be extended to include random waves in future research.

Competing interest The authors have no competing interests to declare that are relevant to the content of this article.

References

Appandairaj R, Vijay KG, Murali K, Chen JT (2024) Oblique wave interaction with dual submerged oscillating buoy as WEC near a partially reflecting wall. Engineering Analysis with Boundary Elements 166: 105822. DOI: 10.1016/j.enganabound.2024.105822

Bautista E, Bahena-Jimenez S, Quesada-Torres A, Méndez F, Arcos E (2022) Interaction between long water waves and two fixed submerged breakwaters of wavy surfaces. Wave Motion 112: 102926. DOI: 10.1016/j.wavemoti.2022.102926

Behera H, Ghosh S (2019) Oblique wave trapping by a surface-piercing flexible porous barrier in the presence of step-type bottoms. Journal of Marine Science and Application 18: 433-443. DOI: 10.1007/s11804-018-0036-2

Behera H, Kaligatla RB, Sahoo T (2015) Wave trapping by porous barrier in the presence of step type bottom. Wave Motion 57: 219-230. DOI: 10.1016/j.wavemoti.2015.04.005

Burke JE (1964) Scattering of surface waves on an infinitely deep fluid. Journal of Mathematical Physics 5(6): 805-819. DOI: 10.1063/1.1704182

Cho IH, Kim MH (2000) Interactions of horizontal porous flexible membrane with waves. Journal of Waterway, Port, Coastal, and Ocean Engineering 126(5): 245-253. DOI: 10.1061/(ASCE)0733-950X(2000)126:5(245)

Cho IH, Kim MH (2008) Wave absorbing system using inclined perforated plates. Journal of Fluid Mechanics 608: 1-20. DOI: 10.1017/S0022112008001845

Choudhary S, Martha SC (2023) Dissipation of incident wave energy by two floating horizontal porous plates over a trench type bottom. Ships and Offshore Structures 19(4): 509-531. DOI: 10.1080/17445302.2023.2186056

Chwang AT (1983) A porous-wavemaker theory. Journal of Fluid Mechanics 132: 395-406. DOI: 10.1017/S0022112083001676

Dai J, Wang CM, Utsunomiya T, Duan W (2018) Review of recent research and developments on floating breakwaters. Ocean Engineering 158: 132-151. DOI: 10.1016/j.oceaneng.2018.03.083

Dalrymple RA, Losada MA, Martin PA (1991) Reflection and transmission from porous structures under oblique wave attack.

Journal of Fluid Mechanics 224: 625-644. DOI: 10.1017/S0022112091001908

Davies AG (1982) The reflection of wave energy by undulations on the seabed. Dynamics of Atmospheres and Oceans 6(4): 207-232. DOI: 10.1016/0377-0265(82)90029-X

Evans DV, Peter MA (2011) Asymptotic reflection of linear water waves by submerged horizontal porous plates. Journal of Engineering Mathematics 69: 135-154. DOI: 10.1007/s10665-009-9355-2

Greene TR, Heins AE (1953) Water waves over a channel of infinite depth. Quarterly of Applied Mathematics 11(2): 201-214. http://www.jstor.org/stable/43634035

Heins AE (1950) Water waves over a channel of finite depth with a submerged plane barrier. Canadian Journal of Mathematics 2: 210-222. DOI: 10.4153/cjm-1950-019-2

Isaacson M, Qu S (1990) Waves in a harbour with partially reflecting boundaries. Coastal Engineering 14(3): 193-214. DOI: 10.1016/0378-3839(90)90024-Q

Kaligatla RB, Tabssum S, Sahoo T (2018) Effect of bottom topography on wave scattering by multiple porous barriers. Meccanica 53: 887-903. DOI: 10.1007/s11012-017-0790-2

Koley S, Kaligatla RB, Sahoo T (2015) Oblique wave scattering by a vertical flexible porous plate. Studies in Applied Mathematics 135(1): 1-34. DOI: 10.1111/sapm.12076

Kumar UV, Saha S, Koley S (2023) A comparative study of wave scattering by non-porous and porous flexible plates in the presence of a submerged porous structure. Meccanica 58: 1329-1346. DOI: 10.1007/s11012-023-01679-w

Leppington FG (1972) On the radiation and scattering of short surface waves. Part 1. Journal of Fluid Mechanics 56(1): 101-119. DOI: 10.1017/S0022112072002216

Liu PLF, Iskandarani M (1991) Scattering of short-wave groups by submerged horizontal plate. Journal of Waterway, Port, Coastal, and Ocean Engineering 117(3): 235-246. DOI: 10.1061/(ASCE)0733-950X(1991)117:3(235)

Liu Y, Li HJ (2014) Analysis of wave performance through pile–rock breakwaters. Proceedings of the Institution of Mechanical Engineers, Part M: Journal of Engineering for the Maritime Environment 228(3): 284-292. DOI: 10.1177/1475090212462951

Liu Y, Li HJ, Li YC (2012) A new analytical solution for wave scattering by a submerged horizontal porous plate with finite thickness. Ocean Engineering 42: 83-92. DOI: 10.1016/j.oceaneng.2012.01.001

Mackay E, Johanning L (2020) Comparison of analytical and numerical solutions for wave interaction with a vertical porous barrier. Ocean Engineering 199: 107032. DOI: 10.1016/j.oceaneng.2020.107032

Mohapatra AK, Sahoo T (2023) Surface gravity wave interaction with a floating dock in the presence of a submerged composite wavy porous plate. Applied Ocean Research 139: 103686. DOI: 10.1016/j.apor.2023.103686

Mondal A, Panda S, Gayen R (2017) Flexural-gravity wave scattering by a circular-arc-shaped porous plate. Studies in Applied Mathematics 138(1): 77-102. DOI: 10.1111/sapm.12137

Neelamani S, Rajendran R (2002) Wave interaction with T-type breakwaters. Ocean Engineering 29(2): 151-175. DOI: 10.1016/S0029-8018(00)00060-3

Nguyen NM, Do Van D, Le DT, Cong SD, Pham NT, Nguyen Q, Tran B, Wright DP, Tanim AH, Anh DT (2022) Wave reduction efficiency for three classes of breakwaters on the coastal Mekong Delta. Applied Ocean Research 129: 103362. DOI: 10.1016/j.apor.2022.103362

Ning DZ, Wang RQ, Zou QP, Teng B (2016) An experimental investigation of hydrodynamics of a fixed OWC Wave Energy Converter. Applied Energy 168: 636-648. DOI: 10.1016/j.apenergy.2016.01.107

Nishad CS, Vijay KG, Neelamani S, Chen JT (2021) Dual BEM for wave scattering by an H-type porous barrier with nonlinear pressure drop. Engineering Analysis with Boundary Elements 131: 280-294. DOI: 10.1016/j.enganabound.2021.06.011

Panduranga K, Koley S, Meylan MH (2023) A hybrid boundary element method based model for wave interaction with submerged viscoelastic plates with an arbitrary bottom profile in frequency and time domain. Physics of Fluids 35(4): 047114. DOI: 10.1063/5.0143412

Patarapanich M (1984) Maximum and zero reflection from submerged plate. Journal of Waterway, Port, Coastal, and Ocean Engineering 110(2): 171-181. DOI: 10.1061/(ASCE)0733-950X(1984)110:2(171)

Patarapanich M, Cheong HF (1989) Reflection and transmission characteristics of regular and random waves from a submerged horizontal plate. Coastal Engineering 13(2): 161-182. DOI: 10.1016/0378-3839(89)90022-7

Pérez-Romero DM, Ortega-Sánchez M, Moñino A, Losada MA (2009) Characteristic friction coefficient and scale effects in oscillatory porous flow. Coastal Engineering 56(9): 931-939. DOI: 10.1016/j.coastaleng.2009.05.002

Rageh OS, Koraim AS, Salem TN (2009) Hydrodynamic efficiency of partially immersed caissons supported on piles. Ocean Engineering 36(14): 1112-1118. DOI: 10.1016/j.oceaneng.2009.06.009

Rezanejad K, Bhattacharjee J, Guedes Soares C (2015) Analytical and numerical study of dual-chamber oscillating water columns on stepped bottom. Renewable Energy 75: 272-282. DOI: 10.1016/j.renene.2014.09.050

Siew PF, Hurley DG (1977) Long surface waves incident on a submerged horizontal plate. Journal of Fluid Mechanics 83(1): 141-151. DOI: 10.1017/S0022112077001098

Sollitt CK, Cross RH (1972) Wave transmission through permeable breakwaters. Coastal Engineering Proceedings, Vancouver, Canada, 1827-1846. DOI: 10.1061/9780872620490.106

Tabssum S, Ramakrishnan B (2024) Oblique wave interaction with flexible plate in ocean of uneven bottom. Journal of Marine Science and Application 23(2): 261-275. DOI: 10.1007/s11804-024-00395-5

Varghese A, Athul Krishna KR, Karmakar D (2024) Wave attenuation due to stratified porous structure with stepped seabed. Journal of Marine Science and Application 23: 844-866. DOI: 10.1007/s11804-024-00407-4

Venkateswarlu V, Karmakar D (2020) Significance of seabed characteristics on wave transformation in the presence of stratified porous block. Coastal Engineering Journal 62(1): 1-22. DOI: 10.1080/21664250.2019.1676366

Venkateswarlu V, Vijay KG, Nishad CS (2021) Iterative dual boundary element analysis of a wavy porous plate near an inclined seawall. Ocean Engineering 235: 109242. DOI: 10.1016/j.oceaneng.2021.109242

Vijay KG, He SY, Zhao Y, Liu Y, Sahoo T (2020) Gravity wave interaction with a submerged wavy porous plate. Ships and Offshore Structures 15(sup1): S123-S133. DOI: 10.1080/17445302.2020.1789034

Vijay KG, Venkateswarlu V, Sahoo T (2021) Bragg scattering of surface gravity waves by an array of submerged breakwaters and a floating dock. Wave Motion 106: 102807. DOI: 10.1016/j.wavemoti.2021.102807

Vishwakarma RD, Karmakar D (2024) Hydrodynamic analysis of different shapes of moored hybrid floating breakwater. Journal of Marine Science and Application 23: 743-761. DOI: 10.1007/

s11804-024-00519-x

Yip TL, Chwang AT (1997) Water wave control by a pitching plate. Journal of Engineering Mechanics 123(8): 800-807. DOI: 10.1061/(ASCE)0733-9399(1997)123:8(800)

Yu X (2002) Functional performance of a submerged and essentially horizontal plate for offshore wave control: A review. Coastal Engineering Journal 44(2): 127-147. DOI: 10.1142/S0578563402000470

Yu X, Chwang AT (1994) Water waves above submerged porous plate. Journal of Engineering Mechanics 120(6): 1270-1282. DOI: 10.1061/(ASCE)0733-9399(1994)120:6(1270)

Yueh CY, Chuang SH, Wen CC (2016) Wave scattering by submerged composite wavy plate breakwaters using a dual BEM. Ocean Engineering 124: 192-203. DOI: 10.1016/j.oceaneng.2016.07.019

Zhang XS, Ma S, Duan WY (2018) A new L type floating breakwater derived from vortex dissipation simulation. Ocean Engineering 164: 455-464. DOI: 10.1016/j.oceaneng.2018.06.059

Zhao Y, Liu Y, Li H (2016) Wave interaction with a partially reflecting vertical wall protected by a submerged porous bar. Journal of Ocean University of China 15: 619-626. DOI: 10.1007/s11802-016-2837-8